Institute of
Sound and Vibration Research

Effect of steady flow distortion on modes propagating in a turbofan intake duct

Internship Report
May 10, 2012

Author:
Ellen Norde
e.norde@student.utwente.nl
Chair Engineering Fluid Dynamics

On behalf of:
University of Twente
Faculty of Engineering Technology
MSc Mechanical Engineering

Supervisors (ISVR):
Prof. Jeremy Astley
Dr. Rie Sugimoto

Supervisor (UT):
Prof.Dr.Ir. Harry Hoeijmakers

UNIVERSITY OF Southampton
Institute of Sound and Vibration Research

UNIVERSITY OF TWENTE.

Abstract

This report contains research into the effect of steady flow distortion on modes propagating in a turbofan intake duct. The motivation for this work is the requirement to predict the effect of flow distortion in modern bypass turbofan aeroengines such that it can be used in noise reduction treatments. A set of analytical and numerical methods for predicting the effect of flow distortion have been developed.

Analytical solutions for a rectangular and annular duct have been derived to find the modal amplitudes in ducts with uniform and nonuniform flow. These solutions are obtained by using a variational formulation of Pridmore-Brown's equation. A direct eigenvalue solver in MATLAB is developed to support the analytical solution and it is demonstrated that flow distortion has a significant effect on propagating modes.

The numerical results are compared to Rolls-Royce data that is obtained from measurements on three different configurations of intake ducts. It is found that there exist similarities between this data and the analytical/numerical model.

Acknowledgments

This report is the result of four months internship in the field of aircraft noise and is part of my master's in Mechanical Engineering at the Engineering Fluid Dynamics Group at the University of Twente. Its realisation would not have been possible without the support of many different people.

First of all, I would like to thank Prof. Jeremy Astley and Dr. Rie Sugimoto for their great support and guidance during my research, and for introducing me into the interesting field of aircraft noise. Secondly, a special thanks to Dr. Andrew Kempton for accommodating me during my two days at Rolls-Royce and to Pete Schwaller for helping me with the data extraction.

It has been a great pleasure to share an office with colleagues from many different backgrounds and nationalities. Thank you for giving me the 'ISVR welcome'! Christian Stoehr and Tiphane Ricoup, thanks for the enjoyable lunches with our never-ending comparison of daily life in England, Germany, France and The Netherlands. I would also like to thank Sue Brindle for helping me to tackle some bureaucratic hurdles.

Last but not least, I want to thank Prof. Harry Hoeijmakers for introducing me at ISVR and for the extensive guidance that I have received since the beginning of my master's.

Finally, I would like to express my gratitude to my parents and friends for their endless support, love and laughter.

Contents

List of Figures

List of Tables

Nomenclature

Latin Symbols

A	Duct cross-sectional area
A_{mn}	Modal amplitude of mode (m, n)
$abcd$	Integers a, b, c and d
c_0	Speed of sound
H_n	Helmholtz number
h	Duct height
h_r	Hub-tip ratio annular duct
J_m	Bessel function of order m (Bessel function of the first kind)
K	Mach weighted acoustic 'stiffness' matrix
k	Free field acoustic wave number
k_z	Axial wave number
k_z^+	Axial wave number positive acoustic modes
k_z^-	Axial wave number negative acoustic modes
L	Duct length
M	Mach weighted acoustic 'mass' matrix
M_0	Flow Mach number
m	Circumferential mode order, $m = [..., -1, 0, 1, ...]$
n	Radial mode order, $n = 1, 2, 3, ...$
p	Pressure, unsteady/acoustic component
p_0	Pressure, mean flow component
p'	Pressure, total unsteady component
$\hat{p}$	Pressure satisfying the convected Helmholtz equation
$Q_{mn}(r)$	Solution to Bessel's equation
q	Modal acoustic power
q_{nm}	Acoustic power of mode (m, n)
r	Average duct radius
r_0	Inner duct radius
r_1	Outer duct radius
S	'Shear' coupling matrix
s	Integer s (= 0,1,2,3)
t	Time
$\mathbf{u}$	Velocity, unsteady/acoustic component
$\mathbf{u}_0$	Velocity, mean flow component
$\mathbf{u}'$	Velocity, total unsteady component
W	Trial function
W_{mn}	Combination of trial functions ϕ_m and ψ_n
w_0	Axial velocity
X	Matrix component
Y_m	Neumann function of order m (Bessel function of the second kind)
Z	Wall impedance
$(\mathbf{e}_x, \mathbf{e}_y, \mathbf{e}_z)$	Cartesian unit vector notation
(r, θ, z)	Cylindrical coordinate system
(x, y, z)	Cartesian coordinate system

Greek Symbols

α_n	n-dependent coefficient, $n\pi/k$
β_m	m-dependent coefficient, $m/\mathbf{r}$
γ	Ratio of specific heats, C_P/C_V
$\Delta_\perp$	Laplacian in cross-section of duct
ϵ	Flow distortion factor
ϵ_n	n-dependent value
Γ	Boundary of A, ∂A
κ_{nm}	Radial wave number
λ	Eigenvalue, modal wave number
$\nabla_\perp$	Gradient operator in cross-section of duct
ρ	Density, unsteady/acoustic component
ρ_0	Density, mean flow component
ρ'	Density, total unsteady component
ω	Angular frequency

Abbreviations

EO	Engine Order
FAA	Federal Aviation Administration
FDAG	Fluid Dynamics and Acoustics Group
ICAO	International Civil Aviation Organisation
ISVR	Institute of Sound and Vibration Research
OGV	Outlet Guide Vane
SPL	Sound Pressure Level
UT	University of Twente
UTC	University Technology Centre

Chapter 1

Introduction

1.1 Institute of Sound and Vibration Research [1]

The Institute of Sound and Vibration Research (ISVR) is one of the leading research centres for acoustics in the world and is part of the University of Southampton. The institute is founded in 1963 and its main activities are graduate-level teaching and research in sound, vibration and related areas. The research is divided into four research groups:

- Dynamics,
- Fluid Dynamics and Acoustics,
- Human Sciences: 'Human Factors Research Unit' and the 'Hearing and Balance Centre',
- Signal Processing and Control.

My internship was fulfilled in the 'Fluid Dynamics and Acoustics Group (FDAG)'. This group is active in three major areas: aeroacoustics of aircraft engines, ultrasonics and underwater acoustics, and noise source imaging and virtual acoustics and has about 20 academic and research staff as well as a large group of research students. The Rolls-Royce University Technology Centre (UTC) in Gas Turbine Noise is also included in this group. The UTC forms part of the global Rolls-Royce research network and undertakes research on all aspects of aircraft noise.

1.2 Rolls-Royce [2]

Rolls-Royce is a global business providing integrated power systems for use on land, at sea and in the air. The company's products in the Civil Aerospace branch are small and large aircraft engines and helicopter engines. Some of the newest large aircraft engines are the Trent 1000, which entered into service on Boeing 787 in 2011, and the Trent XWB for Airbus 350 XWB which just completed its first test flight powering an Airbus A380 in February 2012. The plant in Derby, UK, employs over 11,000 workers and most work in the Civil Aerospace business. The Trent family engines are both designed and manufactured in Derby and their site includes the main module and engine assembly lines, engine test beds as well as manufacturing sites producing a range of components, including turbine blades, fan parts and rotative components. Besides the Civil Aerospace business, Derby is also the centre of the company's nuclear activities and the Submarines business is located there as well.

1.3 Aircraft engine noise

The use of turbojet and turbofan engines in civil aviation from 1960 onwards and the rapid growth of air travel contributed to a considerable increase in noise nuisance. Its effect on passengers and crew inside the aircraft, but especially on residents close to airports made regulation of aircraft noise necessary. The US Federal Aviation Administration (FAA) and the International Civil Aviation Organisation (ICAO) both imposed noise requirements around 1970. These regulations have become more strict and global through the years.
The two main sources of aircraft noise are airframe noise and engine noise [3]. The locations of different

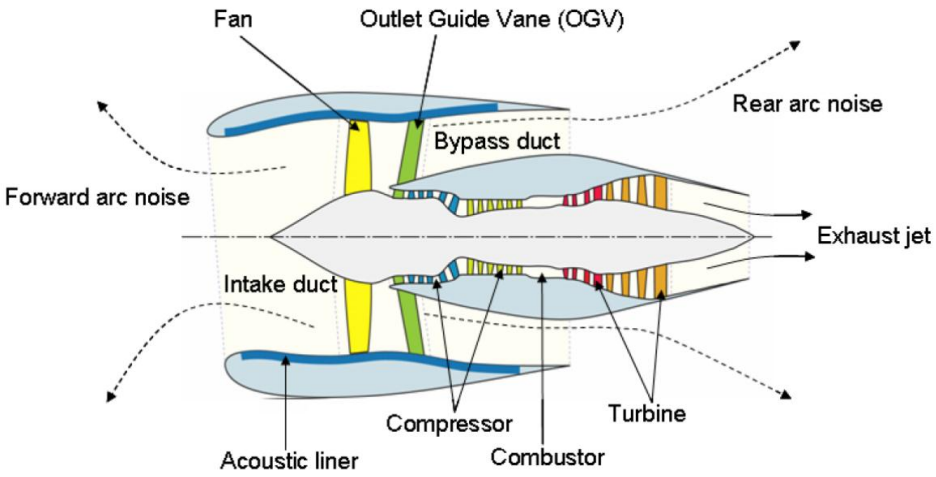

Figure 1.1: High by-pass turbofan engine showing main components and direction of noise radiation [3].

sources of noise on a turbofan engine are shown in Figure 1.1. Noise generated by the fan and outlet guide vanes (OGVs) propagates into the forward and rear arcs through the intake and bypass ducts and is one of the major contributors to the total aircraft noise today [4]. This can be ascribed to the increase in bypass ratios of commercial turbofan aeroengines. The bypass ratio of the engine is defined as the ratio of the air mass flow rate through the bypass duct to the air mass flow rate through the core of the engine. Turbofan noise is for instance generated by unsteady flow in the fan, compressor, and turbine.
A very effective way of reducing fan noise is the use of acoustic treatment within the intake and bypass ducts. The usual way of doing this is to cover the duct surface with locally reacting acoustic absorbers, or liners (see Figure 1.1).

1.4 Outline

The aim of this internship is to study the effect of steady flow distortion on modes propagating in a turbofan intake duct. Duct modes are terms in the series expansion that form the solution of the acoustic problem. A brief summary of this acoustic theory is presented in Chapter 2. This research is started from the analytical derivation of the acoustics in a simple duct geometry before it is improved to a geometry which is a better representation of the real turbofan intake and this is also explained in Chapter 2. The effect of flow distortion is studied in three levels: uniform flow and non-uniform flow, where the latter is at first approximated by a linear distortion and followed by a fully nonlinear distortion of the flow. In Chapter 3 and 4 the analytical solution for a rectangular and an annular duct, respectively, are presented for these three flow cases. A MATLAB code is written to assess the results for the rectangular duct and these results are shown in Chapter 5.
In Chapter 6 the results for the rectangular geometry are compared to Rolls-Royce data. These data are obtained from mode detection measurements of a particular intake for two different geometries and either hard-walled or lined duct surfaces. Finally, overall conclusions and recommendations for future work are presented in Chapter 7.

Chapter 2

Duct acoustics

2.1 Duct geometry

A sketch of a turbofan engine intake is given in Figure 2.1a. This intake can be approximated by an annular duct model, Figure 2.1b, where the dimensions are taken from the fan plane of the engine intake. Here r the average radius, $r = (r_1 + r_0)/2$, where r_1 and r_0 are the outer and inner radius, respectively. This annular airway is 'unwrapped' to give a rectangular duct at the same height ($h = r_1 - r_0$) and same cross-sectional area: $A = 2\pi r h = \pi(r_1^2 - r_0^2)$. This result is shown in Figure 2.2.
Furthermore, it is assumed that the axial velocity w_0 in the annular case is $w_0 = w_0(\theta)$. This corresponds to $w_0 = w_0(x)$ in the 'unwrapped' rectangular duct case. w_0 must repeat itself at $x = L = 2\pi r$ to satisfy periodic boundary conditions.

The boundary conditions for a hard-walled inner/outer surface of the two-dimensional rectangular duct case are

$$\frac{\partial q}{\partial y} = 0 \quad , \quad y = 0, h, \tag{2.1}$$

where q is the modal acoustic power.

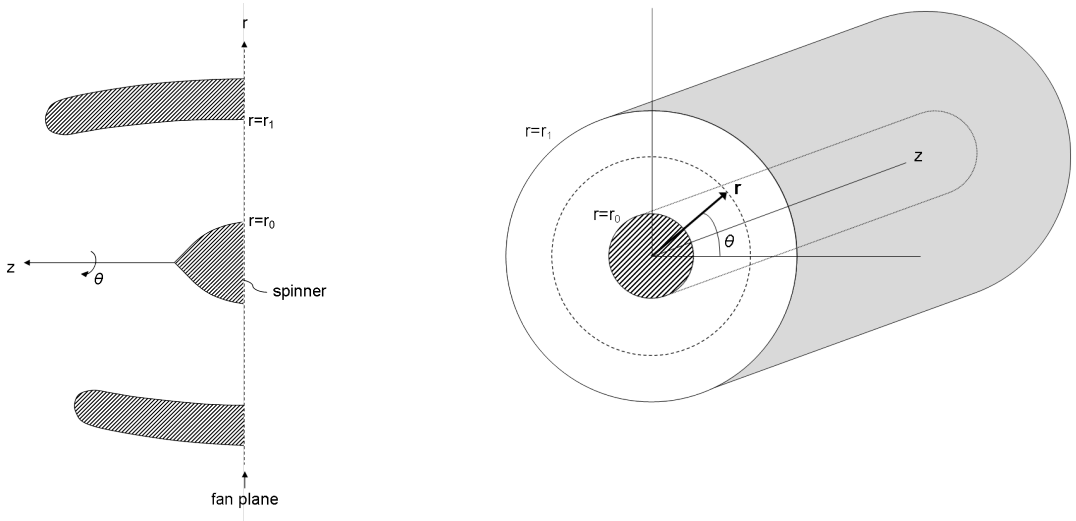

(a) Side view of a turbofan engine intake in cylindrical coordinates (r, θ, z).

(b) Fan plane of uniform annular duct model in cylindrical coordinates (r, θ, z).

Figure 2.1: Sketches of turbofan engine intake versus annular duct model.

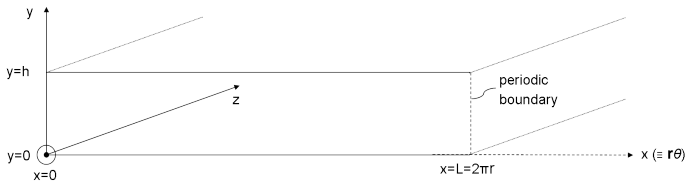

Figure 2.2: Sketch of a rectangular duct in Cartesian coordinates (x, y, z).

2.2 Acoustic equations

The necessary equations can be derived starting from the governing equations in non-dimensional form for the isentropic motion of a non-viscous, non-heat-conducting perfect gas

$$\text{Continuity} \qquad \frac{\partial \rho'}{\partial t} + \nabla \cdot (\rho' \mathbf{u}') = 0, \tag{2.2}$$

$$\text{Momentum} \qquad \frac{\partial \mathbf{u}'}{\partial t} + (\mathbf{u}' \cdot \nabla)\mathbf{u}' = -\frac{1}{\rho'}\nabla p', \tag{2.3}$$

$$\text{Equation of state} \qquad p' = \frac{1}{\gamma}\rho'^{\gamma}, \tag{2.4}$$

where ρ, p, $\mathbf{u}$, t and γ are the density, pressure, velocity, time and ratio of specific heats (C_P/C_V), respectively. The acoustic equations can be expressed as the sum of acoustic perturbations ρ', p' and $\mathbf{u}'$ and the mean state, ρ_0, p_0 and $\mathbf{u}_0$

$$\begin{aligned} \rho' &= \rho_0 + \rho, \\ p' &= p_0 + p, \\ \mathbf{u}' &= \mathbf{u}_0 + \mathbf{u}. \end{aligned}$$

Ignoring the second-order and higher order terms of the perturbations now gives the acoustic field equations

$$\text{Acoustic continuity:} \qquad \frac{\partial \rho}{\partial t} + \nabla \cdot (\rho_0 \mathbf{u} + \mathbf{u}_0 \rho) = 0, \tag{2.5}$$

$$\text{Acoustic momentum:} \qquad \frac{\partial \mathbf{u}}{\partial t} + \mathbf{u}_0 \cdot \nabla \mathbf{u} + \frac{1}{\rho_0}\nabla p + \mathbf{u} \cdot \nabla \mathbf{u}_0 - \frac{1}{\gamma p_0 \rho_0} p \nabla p_0 = 0, \tag{2.6}$$

$$\text{Acoustic equation of state:} \qquad p = \gamma \frac{p_0}{\rho_0}\rho = c_0^2 \rho, \tag{2.7}$$

where c_0 is the speed of sound.

Chapter 3

Rectangular duct

3.1 Rectangular uniform duct with mean flow [6]

Equations (2.5) to (2.7) are the appropriate equations in case of the uniform rectangular duct of Figure 2.2 carrying a mean flow which is axially uniform but non-uniform in the $x-$direction. For this case the equations are restricted to the situation where ρ_0 and p_0 are constant ($\rho_0 = 1$ and $p_0 = 1$) and $\mathbf{u}_0 = w_0(x)\mathbf{e}_z$

$$\frac{1}{c_0^2}\frac{\partial p}{\partial t} + \frac{w_0}{c_0^2}\frac{\partial p}{\partial z} + \nabla \cdot \mathbf{u} = 0, \tag{3.1}$$

$$\frac{\partial \mathbf{u}}{\partial t} + w_0\frac{\partial \mathbf{u}}{\partial z} + \nabla p + \frac{\mathrm{d}w_0}{\mathrm{d}x}u\mathbf{e}_z = 0, \tag{3.2}$$

where

$$\mathbf{u} = u\mathbf{e}_x + v\mathbf{e}_y + w\mathbf{e}_z.$$

Taking the divergence of the momentum equation gives

$$\nabla \cdot \left[\frac{\partial \mathbf{u}}{\partial t} + w_0\frac{\partial \mathbf{u}}{\partial z} + \nabla p + \frac{\mathrm{d}w_0}{\mathrm{d}x}u\mathbf{e}_z\right] = \left(\frac{\partial}{\partial t} + w_0\frac{\partial}{\partial z}\right)(\nabla \cdot \mathbf{u}) + \nabla^2 p + 2\mathbf{e}_z\frac{\mathrm{d}w_0}{\mathrm{d}x}\frac{\partial u}{\partial z} = 0. \tag{3.3}$$

Substitution of the continuity equation, Equation (3.1), into this equation now leads to

$$-\frac{1}{c_0^2}\left(\frac{\partial}{\partial t} + w_0\frac{\partial}{\partial z}\right)^2 p + \nabla^2 p + 2\mathbf{e}_z\frac{\mathrm{d}w_0}{\mathrm{d}x}\frac{\partial u}{\partial z} = 0. \tag{3.4}$$

The radial acoustic particle velocity u is eliminated by forming the axial partial derivative of the radial momentum equation to give [5]

$$\left(\frac{\partial}{\partial t} + w_0\frac{\partial}{\partial z}\right)\frac{\partial u}{\partial z} = -\frac{\partial^2 p}{\partial x \partial z}. \tag{3.5}$$

Substitution of Equation (3.5) into Equation (3.4) results in a single third order differential equation in pressure given by

$$\frac{1}{c_0^2}\left(\frac{\partial}{\partial t} + w_0\frac{\partial}{\partial z}\right)^3 p = \left(\frac{\partial}{\partial t} + w_0\frac{\partial}{\partial z}\right)\nabla^2 p - 2\frac{\mathrm{d}w_0}{\mathrm{d}x}\frac{\partial^2 p}{\partial x \partial z}. \tag{3.6}$$

To solve this equation, solutions are sought of the form

$$p(x, y, z, t) = \hat{p}(x, y, z)e^{i\omega t},$$

where ω is a prescribed frequency. The resulting equation for $\hat{p}(x, y, z)$ is

$$\frac{1}{c_0^2}\left(i\omega + w_0\frac{\partial}{\partial z}\right)^3 \hat{p} = \left(i\omega + w_0\frac{\partial}{\partial z}\right)\nabla^2 \hat{p} - 2\frac{\mathrm{d}w_0}{\mathrm{d}x}\frac{\partial^2 \hat{p}}{\partial x \partial z}. \tag{3.7}$$

This equation is equal to Pridmore-Brown's equation given as Equation (1) in [8]

$$\left(i\omega + w_0\frac{\partial}{\partial z}\right)\left[\frac{1}{c_0^2}\left(i\omega + w_0\frac{\partial}{\partial z}\right)^2 \hat{p} - \Delta\hat{p}\right] + 2\frac{\partial}{\partial z}(\nabla_\perp w_0 \cdot \nabla_\perp \hat{p}) = 0, \tag{3.8}$$

where $\nabla_\perp$ is the gradient operator in the cross-section of the duct.
Now traveling wave solutions are sought of the form

$$\hat{p}(x, y, z) = q(x, y)e^{-ik\lambda z},$$

where $k = \omega/c_0$ is the free-field wave number and $k\lambda = k_z$ is the axial wave number of the mode. From Equation (3.7) the equation for q can be derived

$$\left(i\omega + w_0\frac{\partial}{\partial z}\right)^3 \left[q(x, y)e^{-ik\lambda z}\right] = \left(i\omega + w_0\frac{\partial}{\partial z}\right)\nabla^2\left[q(x, y)e^{-ik\lambda z}\right] - 2\frac{\mathrm{d}w_0}{\mathrm{d}x}\frac{\partial^2\left[q(x, y)e^{-ik\lambda z}\right]}{\partial x \partial z}$$
$$\implies \frac{1}{c_0^2}\left(-i\omega^3 + 3i\lambda\omega^2 k w_0 - 3i\lambda^2\omega k^2 w_0^2 + i\lambda^3 k^3 w_0^3\right) q = (i\omega - i\lambda k w_0)\nabla^2 q + 2i\lambda k\frac{\mathrm{d}w_0}{\mathrm{d}x}\frac{\partial q}{\partial x}.$$

Multiplying by i and using the definitions for k and the flow Mach number $M_0 = w_0/c_0$ gives

$$\left(k^2 - 3\lambda k^2 M_0 + 3\lambda^2 k^2 M_0^2 - \lambda^3 k^2 M_0^3\right) q = (-1 + \lambda M_0)\nabla^2 q - 2\lambda\frac{\mathrm{d}M_0}{\mathrm{d}x}\frac{\partial q}{\partial x}.$$

Finally, this can be rewritten to

$$(1 - \lambda M_0)[\Delta_\perp q + k^2[(1 - \lambda M_0)^2 - \lambda^2]q] + 2\lambda[\nabla_\perp M_0 \cdot \nabla_\perp q] = 0, \quad \text{with} \quad \Delta_\perp \equiv \frac{\partial}{\partial x^2} + \frac{\partial}{\partial y^2}, \tag{3.9}$$

which is equal to Equation (3) in [8]. For the two-dimensional rectangular duct (see Figure 2.2) this equation is equal to

$$(1 - \lambda M_0)\left[\frac{\partial^2 q}{\partial x^2} + \frac{\partial^2 q}{\partial y^2} + k^2[(1 - \lambda M_0)^2 - \lambda^2]q\right] + 2\lambda\left[\frac{\partial M_0}{\partial x}\frac{\partial q}{\partial x}\right] = 0. \tag{3.10}$$

3.2 Uniform flow

For uniform flow M_0 is constant or $\mathrm{d}M_0/\mathrm{d}x = 0$. Equation (3.10) then changes to

$$(1 - \lambda M_0)\left[\frac{\partial^2 q}{\partial x^2} + \frac{\partial^2 q}{\partial y^2} + k^2[(1 - \lambda M_0)^2 - \lambda^2]q\right] = 0, \tag{3.11}$$

which has solutions

$$\lambda = \frac{1}{M_0} \quad \text{or} \quad \frac{\partial^2 q}{\partial x^2} + \frac{\partial^2 q}{\partial y^2} + k^2\left[(1 - \lambda M_0)^2 - \lambda^2\right] q = 0.$$

It is observed that hydrodynamic (rotational) disturbances and acoustic (irrotational) disturbances can be separated in uniform flow. Hydrodynamic modes are convected with the flow. At first, only acoustic modes are considered and solutions are sought of the form

$$\begin{aligned} q_{mn} &= A_{mn}\cos\frac{n\pi y}{h}e^{im\{\frac{2\pi x}{L}\}} \\ &= A_{mn}\cos\frac{n\pi y}{h}e^{im(\frac{x}{\mathbf{r}})} \\ &= A_{mn}\cos(\alpha_n y)e^{i\beta_m x} \quad , \quad \alpha_n = \frac{(n-1)\pi}{h}, \quad \beta_m = \frac{m}{\mathbf{r}}, \end{aligned}$$

where A_{mn} is the modal amplitude of mode (m, n) and m and n are the circumferential and radial mode orders, respectively, where $m = [..., -1, 0, 1, ...]$ and $n = 1, 2, 3....$ It can be seen that the *cosine*-part satisfies the boundary conditions at $y = 0, h$ and the *exponential*-part satisfies the periodicity over $[0, L]$. Substitution of q into the acoustic solution of Equation (3.11) now gives

$$-\alpha_n^2 - \beta_m^2 + k^2\left[(1 - \lambda M_0)^2 - \lambda^2\right] = 0, \tag{3.12}$$

which is equal to a simple quadratic equation

$$(M_0^2-1)k^2\lambda^2 - 2k^2M_0\lambda + k^2 - \alpha_n^2 - \beta_m^2 = 0,$$

with roots following from the quadratic formula

$$\begin{aligned}\lambda &= \frac{2k^2M_0 \pm \sqrt{4k^4M_0^2 - 4k^2(M_0^2-1)(k^2-\alpha_n^2-\beta_m^2)}}{2k^2(M_0^2-1)} \\ &= \frac{k^2M_0 \pm \sqrt{k^4M_0^2 - k^2(M_0^2-1)(k^2-\alpha_n^2-\beta_m^2)}}{k^2(M_0^2-1)} \\ \implies \lambda k &= \frac{kM_0}{(M_0^2-1)} \pm \frac{\sqrt{k^2+(M_0^2-1)(\alpha_n^2+\beta_m^2)}}{(M_0^2-1)}. \end{aligned} \tag{3.13}$$

Cut-on and cut-off modes

If for a given mode the axial wave number is purely real, the mode is propagating (cut-on). When the axial wave number has a non-zero imaginary part, the mode is evanescent (cut-off) [3]. Cut-off modes decay with distance and carry no acoustic power [6]. From Equation (3.13) it is clear that modes are cut-on if

$$k^2 > (1-M_0^2)[\alpha_n^2+\beta_m^2],$$

and cut-off if

$$k^2 < (1-M_0^2)[\alpha_n^2+\beta_m^2].$$

Plotting modes

In Figure 3.1 the axial wave numbers $k_z(=k\lambda)$ are plotted for the first 20 radial (n) modes and the values are given in Table 3.1. In this case the values for the Helmholtz number, flow Mach number and geometry of the duct are chosen similar to the ones in [8]:

$$M_0 = 0.4; \quad H_n = kh = 15; \quad r_1 = 1 \text{ m}; \quad r_0 = 0.7 \text{ m}; \quad h = r_1 - r_0 = 0.3 \text{ m}.$$

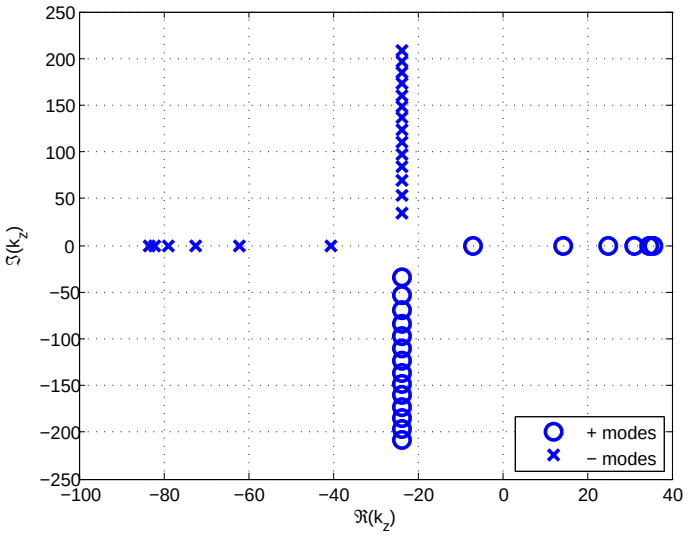

Figure 3.1: First 20 radial modes for a rigid, rectangular duct with uniform flow and $m = 0$, $M_0 = 0.4$, $H_n = kh = 15$, $h = 0.3$.

Table 3.1: Positive and negative modes for $[1, 20]$, $m = 0$, $M_0 = 0.4$, $H_n = kh = 15$, $h = 0.3$.

n	Negative modes	Positive modes
1	-83.33	35.71
2	-82.22	34.61
3	-78.77	31.15
4	-72.47	24.85
5	-61.94	14.32
6	-40.52	-7.097
7	-23.81 + 34.01i	-23.81 - 34.01i
8	-23.81 + 53.42i	-23.81 - 53.42i
9	-23.81 + 69.37i	-23.81 - 69.37i
10	-23.81 + 83.85i	-23.81 - 83.85i
11	-23.81 + 97.53i	-23.81 - 97.53i
12	-23.81 + 110.7i	-23.81 - 110.7i
13	-23.81 + 123.5i	-23.81 - 123.5i
14	-23.81 + 136.1i	-23.81 - 136.1i
15	-23.81 + 148.5i	-23.81 - 148.5i
16	-23.81 + 160.7i	-23.81 - 160.7i
17	-23.81 + 172.9i	-23.81 - 172.9i
18	-23.81 + 184.9i	-23.81 - 184.9i
19	-23.81 + 196.9i	-23.81 - 196.9i
20	-23.81 + 208.8i	-23.81 - 208.8i

Equation (3.13) is solved using Newton-Raphson method. The eigenvalue problem yields a set of positive modes with wave numbers k_z^+ and a set of negative modes with wave numbers k_z^-. The positive acoustic modes are propagating downstream, while the negative acoustic modes are propagating upstream and they are distinguished by using two properties of modes. The first one is that the amplitude of the acoustic perturbations should decrease away from the source. Therefore, the sign of $\Im(k_z)$ indicates the direction of propagation of the mode: $\Im(k_z) < 0$ for positive modes and $\Im(k_z) > 0$ for negative modes. For real values of k_z the modes are propagating in the positive direction if $k_z > kM_0/(M_0^2-1)$ and in the negative direction if $k_z < kM_0/(M_0^2-1)$ [8], where $kM_0/(M_0^2-1)$ is the distance between the real part of the imaginary mode values (the vertical 'line' of the cross-like plot in Figure 3.1) and the imaginary axis at $\Re(k_z) = 0$.

3.3 Non-uniform flow

3.3.1 Flow distortion

In the non-uniform flow case it holds that $\mathrm{d}M_0/\mathrm{d}\theta \neq 0$. For the flow distortion the following case is being considered

$$\begin{aligned} M_0(x) &= M_0\left(1+\epsilon\cos\beta_1 x\right) \\ &= M_0\left(1+\frac{\epsilon}{2}\left(e^{i\beta_1 x}+e^{-i\beta_1 x}\right)\right), \\ \text{so } \frac{\mathrm{d}M_0}{\mathrm{d}x} &= \frac{1}{2}i\beta_1\epsilon M_0\left(e^{i\beta_1 x}+e^{-i\beta_1 x}\right). \end{aligned}$$

Figure 3.2 shows the particulars of this distortion for the rectangular duct.

The flow distortion in linearly approximated if only values of ϵ are retained and higher orders are left out. Otherwise, the flow distortion is fully nonlinear in ϵ.

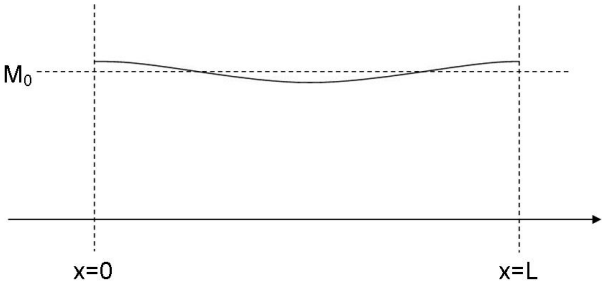

Figure 3.2: Flow distortion in a rectangular duct.

3.3.2 Variational formulation

In Equation (5) of [8] the eigenvalue problem for a lined duct is recasted as a variational formulation with eigenvalue λ and eigenvector q

$$\begin{aligned} &\int_A \left[(1-\lambda M_0)\left[k^2\overline{W}\left[(1-\lambda M_0)^2-\lambda^2\right]q-\nabla_\perp\overline{W}\cdot\nabla_\perp q\right]+3\lambda\overline{W}\nabla_\perp M_0\cdot\nabla_\perp q\right]\mathrm{d}A \\ &\quad+\oint_\Gamma \overline{W}\frac{\rho_0 c_0 k}{iZ}(1-\lambda M_0)^3 q\mathrm{d}\Gamma = 0, \quad \forall W. \end{aligned} \tag{3.14}$$

This result is obtained by multiplying Equation (3.9) by an arbitrary function W, integrating over the domain A and incorporating the boundary condition for a lined duct wall. Here $\Gamma = \partial A$ is the boundary of A and Z is the wall impedance which can vary arbitrarily around the duct wall but which is uniform in the axial direction. In case of a hard-walled duct Equation (3.14) becomes

$$\begin{aligned} &\int_A \left[(1-\lambda M_0)\left[k^2\overline{W}\left[(1-\lambda M_0)^2-\lambda^2\right]q-\nabla_\perp\overline{W}\cdot\nabla_\perp q\right]+3\lambda\overline{W}\nabla_\perp M_0\cdot\nabla_\perp q\right]\mathrm{d}A = 0 \\ &\implies \int_A \left(1-3\lambda M_0+3\lambda^2M_0^2-\lambda^3M_0^3-\lambda^2+\lambda^3M_0\right)k^2\overline{W}q\mathrm{d}A \\ &\quad+\int_A 3\lambda\overline{W}\nabla_\perp M_0\cdot\nabla_\perp q-(1-\lambda M_0)\nabla_\perp\overline{W}\cdot\nabla_\perp q\mathrm{d}A = 0, \end{aligned} \tag{3.15}$$

and solutions are sought of the form

$$\begin{aligned} q &= \sum A_{mn} \cos \frac{n\pi y}{k} e^{im\frac{2\pi x}{L}} \\ &= \sum A_{mn} \cos(\alpha_n y) e^{i\beta_m x} \\ &= \sum A_{mn} \underbrace{\psi_n(y)\phi_m(x)}_{W_{mn}}. \end{aligned}$$

Now define

$$M^{(s)}_{abcd} = \int_A M^s \overline{W}_{ab} W_{cd} \mathrm{d}A, \tag{3.16a}$$

$$K^{(s)}_{abcd} = \int_A M^s \nabla_\perp \overline{W}_{ab} \cdot \nabla_\perp W_{cd} \mathrm{d}A, \tag{3.16b}$$

$$S_{abcd} = \int_A \overline{W}_{ab} \nabla_\perp M \cdot \nabla_\perp W_{cd} \mathrm{d}A, \tag{3.16c}$$

for $s = 0, 1, 2, 3$. When these expressions are substituted into the variational statement, Equation (3.15), this leads to

$$\left(M^0 - 3\lambda M^1 + 3\lambda^2 M^2 - \lambda^3 M^3 - \lambda^2 M^0 + \lambda^3 M^1\right) k^2 + 3\lambda S - (K^0 - \lambda K^1) = 0,$$

and an algebraic eigenvalue problem for λ is obtained of the form

$$X_{abcd} A_{mn} = \left(X_0 + \lambda X_1 + \lambda^2 X_2 + \lambda^3 X_3\right) A_{mn} = 0, \tag{3.17}$$

where $X_0, ..., X_3$ are given by

$$\begin{aligned} X_0 &= k^2 M^0 - K^0, \\ X_1 &= -3k^2 M^1 + K^1 + 3S, \\ X_2 &= 3k^2 M^2 - k^2 M^0, \\ X_3 &= -k^2 M^3 + k^2 M^1. \end{aligned}$$

Working out M^2 and M^3 leads to

$$\begin{aligned} M^2 &= M_0^2 \left(1 + 2\epsilon \cos\beta_1 x + \epsilon^2 \cos^2 \beta_1 x\right) \\ &= M_0^2 \left(1 + \frac{\epsilon^2}{2} + 2\epsilon \cos\beta_1 x + \frac{\epsilon^2}{2} \cos 2\beta_1 x\right), \\ M^3 &= M_0^3 \left(1 + \frac{\epsilon^2}{2} + 2\epsilon \cos\beta_1 x + \frac{\epsilon^2}{2} \cos 2\beta_1 x\right) (1 + \epsilon \cos\beta_1 x) \\ &= M_0^3 \left(\left(1 + \frac{\epsilon^2}{2}\right) + \left(3\epsilon + \frac{\epsilon^3}{2}\right) \cos\beta_1 x + 2\epsilon^2 \cos^2 \beta_1 x + \frac{\epsilon^3}{2} \cos 2\beta_1 x \cos\beta_1 x + \frac{\epsilon^2}{2} \cos 2\beta_1 x\right) \\ &= M_0^3 \left(\left(1 + \frac{3\epsilon^2}{2}\right) + \left(3\epsilon + \frac{3\epsilon^3}{4}\right) \cos\beta_1 x + \frac{3\epsilon^2}{2} \cos 2\beta_1 x + \frac{\epsilon^3}{4} \cos 3\beta_1 x\right). \end{aligned}$$

Orthogonality

Before continuing the derivation, a few orthogonality relations are brought up

$$
\begin{aligned}
\int_0^h \cos\alpha_n y \cos\alpha_m y \mathrm{d}y &= \begin{cases} h & \text{if} \quad m=n=0 \\ \frac{h}{2} & \text{if} \quad m=n\neq 0 \\ 0 & \text{if} \quad m\neq n \end{cases}, \\
\int_0^h \sin\alpha_n y \sin\alpha_m y \mathrm{d}y &= \begin{cases} h & \text{if} \quad m=n=0 \\ \frac{h}{2} & \text{if} \quad m=n\neq 0 \\ 0 & \text{if} \quad m\neq n \end{cases}, \\
\int_0^L e^{-i\beta_m x} e^{i\beta_n x} \mathrm{d}x &= \left.\begin{cases} L & \text{if} \quad m=-n \\ 0 & \text{if} \quad m\neq -n \end{cases}\right\} = L\delta_{m,n}, \\
\int_0^L e^{-i\beta_m x} \cos\beta_n x \mathrm{d}x &= \left.\begin{cases} \frac{1}{2}L & \text{if} \quad m=-n \\ \frac{1}{2}L & \text{if} \quad m=+n \\ 0 & \text{if} \quad \text{otherwise} \end{cases}\right\} = \frac{L}{2}\left(\delta_{m,-n}+\delta_{m,n}\right), \\
\int_0^L e^{-i\beta_m x} \sin\beta_n x \mathrm{d}x &= = \frac{L}{2i}\left(\delta_{m,n}-\delta_{m,-n}\right).
\end{aligned}
\tag{3.18}
$$

3.3.3 Linearly distorted mean flow

For a linear approximation of the distorted flow only the linear terms in ϵ are retained. Working out the M, K and S terms from Equation (3.16) for $b=d=n$ is fixed and by using the obtained expressions for M^2 and M^3 and the integrals relations in Equation (3.18) now gives

$$
\begin{aligned}
M^0_{n,ac} &= \epsilon_n h \left[\int_0^L e^{-i\beta_a x} e^{+i\beta_c x} \mathrm{d}x\right] \\
&= \epsilon_n h L \delta_{a,c}, \\
M^1_{n,ac} &= \epsilon_n h \left[M_0 \int_0^L e^{-i\beta_a x} e^{+i\beta_c x} \left[1+\frac{\epsilon}{2}\left(e^{i\beta_1 x}+e^{-i\beta_1 x}\right)\right] \mathrm{d}x\right] \\
&= \epsilon_n h L M_0 \left[\delta_{a,c}+\frac{\epsilon}{2}\left(\delta_{a,c+1}+\delta_{a,c-1}\right)\right], \\
M^2_{n,ac} &= \epsilon_n h L M_0^2 \left[\delta_{a,c}+\epsilon\left(\delta_{a,c+1}+\delta_{a,c-1}\right)\right], \\
M^3_{n,ac} &= \epsilon_n h L M_0^3 \left[\delta_{a,c}+\frac{3\epsilon}{2}\left(\delta_{a,c+1}+\delta_{a,c-1}\right)\right], \\
K^0_{n,ac} &= \int_A \left(\alpha_b\alpha_d \sin\alpha_b y \sin\alpha_d y e^{-i\beta_a x} e^{+i\beta_c x} + \cos\alpha_b y \cos\alpha_d y (-i\beta_a)(+i\beta_c) e^{-i\beta_a x} e^{+i\beta_c x}\right) \mathrm{d}A \\
&= \epsilon_n h \left[\int_0^L \left(\alpha_n^2 + (-i\beta_a)(+i\beta_c)\right) e^{-i\beta_a x} e^{+i\beta_c x} \mathrm{d}x\right] \\
&= \epsilon_n h L \left(\alpha_n^2+\beta_a\beta_c\right)\delta_{a,c}, \\
K^1_{n,ac} &= \epsilon_n h \left[M_0 \int_0^L \left[1+\frac{\epsilon}{2}\left(e^{i\beta_1 x}+e^{-i\beta_1 x}\right)\right]\left[\alpha_n^2+(-i\beta_a)(+i\beta_c)\right] e^{-i\beta_a x} e^{+i\beta_c x} \mathrm{d}x\right] \\
&= \epsilon_n h L M_0 \left(\alpha_n^2+\beta_a\beta_c\right)\left[\delta_{a,c}+\frac{\epsilon}{2}\left(\delta_{a,c+1}+\delta_{a,c-1}\right)\right], \\
S_{n,ac} &= \epsilon_n h \left[\int_0^L e^{-i\beta_a x} \frac{\partial M}{\partial x} (+i\beta_c) e^{+i\beta_c x} \mathrm{d}x\right] \\
&= \epsilon_n h \left[\int_0^L e^{-i\beta_a x} e^{+i\beta_c x} \beta_c \left[-M_0\epsilon\beta_1 \frac{1}{2}\left(e^{i\beta_1 x}-e^{-i\beta_1 x}\right)\right] \mathrm{d}x\right] \\
&= -\frac{\epsilon}{2}\epsilon_n h L M_0 \beta_c \beta_1 \left(\delta_{a,c+1}-\delta_{a,c-1}\right),
\end{aligned}
$$

where

$$
\epsilon_n = \begin{cases} 1 & \text{if } n=0 \\ \frac{1}{2} & \text{if } n\neq 0. \end{cases}
$$

3.3.4 Nonlinearly distorted mean flow

The expressions for M^2 and M^3 have to be revised for the case of nonlinearly distorted flow because nonlinear terms in ϵ have to be taken into account as well. This gives for M^2

$$\begin{aligned}
M^2_{n,ac} &= \int_A M_0^2 \left(1 + \frac{\epsilon^2}{2} + 2\epsilon\cos\beta_1 x + \frac{\epsilon^2}{2}\cos 2\beta_1 x\right) \cos\alpha_b y e^{-i\beta_a x} \cos\alpha_d y e^{+i\beta_c x} \mathrm{d}A \\
&= \epsilon_n h M_0^2 \int_0^L \left[1 + \frac{\epsilon^2}{2} + \epsilon\left(e^{i\beta_1 x} + e^{-i\beta_1 x}\right) + \frac{\epsilon^2}{4}\left(e^{2i\beta_x} + e^{-2i\beta_1 x}\right)\right] e^{-i\beta_a x} e^{+i\beta_c x} \mathrm{d}x \\
&= \epsilon_n h L M_0^2 \left[\left(1 + \frac{\epsilon^2}{2}\right)\delta_{a,c} + \epsilon\left[\delta_{a,c+1} + \delta_{a,c-1}\right] + \frac{\epsilon^2}{4}\left[\delta_{a,c+2} + \delta_{a,c-2}\right]\right],
\end{aligned}$$

and for M^3

$$\begin{aligned}
M^3_{n,ac} &= \int_A M_0^3 \left[\left(1 + \frac{3\epsilon^2}{2}\right) + \left(3\epsilon + \frac{3\epsilon^3}{4}\right)\cos\beta_1 x + \frac{3\epsilon^2}{2}\cos 2\beta_1 x + \frac{\epsilon^3}{4}\cos 3\beta_1 x\right] \\
&\qquad \times \cos\alpha_b y e^{-i\beta_q x} \cos\alpha_d y e^{+i\beta_s x} \mathrm{d}A \\
&= \epsilon_n h L M_0^3 \left[\left(1 + \frac{3\epsilon^2}{2}\right)\delta_{a,c} + \left(\frac{3\epsilon}{2} + \frac{3\epsilon^2}{8}\right)\left[\delta_{a,c+1} + \delta_{a,c-1}\right] + \frac{3\epsilon^2}{4}\left[\delta_{a,c+2} + \delta_{a,c-2}\right]\right. \\
&\qquad \left. + \frac{\epsilon^3}{8}\left[\delta_{a,c+3} + \delta_{a,c-3}\right]\right].
\end{aligned}$$

These expressions influence only the X_2 and X_3 terms in the algebraic equation, Equation (4.13)

$$\begin{aligned}
X_2 &= 3k^2M^2 - k^2M^0 \\
&= 3\epsilon_n h k^2 L M_0^2 \left[\left(1 + \frac{\epsilon^2}{2}\right)\delta_{a,c} + \epsilon\left[\delta_{a,c+1} + \delta_{a,c-1}\right] + \frac{\epsilon^2}{4}\left[\delta_{a,c+2} + \delta_{a,c-2}\right]\right] \\
&= \epsilon_n h L \delta_{a,c}\left(3k^2M_0^2 + \frac{3\epsilon^2}{2}k^2M_0^2 - k^2\right) + \epsilon_n h L\left[\delta_{a,c+1} + \delta_{a,c-1}\right]\left(3\epsilon k^2 M_0^2\right) \\
&\quad + \epsilon_n h L\left[\delta_{a,c+2} + \delta_{a,c-2}\right]\left(\frac{3\epsilon^2}{4}k^2M_0^2\right), \\
X_3 &= -k^2M^3 + k^2M^1 \\
&= \epsilon_n h k^2 L M_0^3 \left[\left(1 + \frac{3\epsilon^2}{2}\right)\delta_{a,c} + \left(\frac{3\epsilon}{2} + \frac{3\epsilon^2}{8}\right)\left[\delta_{a,c+1} + \delta_{a,c-1}\right] + \frac{3\epsilon^2}{4}\left[\delta_{a,c+2} + \delta_{a,c-2}\right]\right. \\
&\quad \left. + \frac{\epsilon^3}{8}\left[\delta_{a,c+3} + \delta_{a,c-3}\right]\right] \\
&= \epsilon_n h L \delta_{a,c}\left(-k^2M_0^3 - \frac{3\epsilon^2}{2}k^2M_0^3 + k^2M_0\right) + \epsilon_n h L\left[\delta_{a,c+1} + \delta_{a,c-1}\right]\left(-\frac{3\epsilon}{2}k^2M_0^3 - \frac{3\epsilon^2}{8}k^2M_0^3 + \frac{\epsilon}{2}k^2M_0\right) \\
&\quad + \epsilon_n h L\left[\delta_{a,c+2} + \delta_{a,c-2}\right]\left(-\frac{3\epsilon^2}{4}k^2M_0^3\right) + \epsilon_n h L\left[\delta_{a,c+3} + \delta_{a,c-3}\right]\left(-\frac{\epsilon^3}{8}k^2M_0^3\right).
\end{aligned}$$

3.4 Variational formulation uniform mean flow

In order to check the variational formulation for the rectangular approximation of the duct, the uniform flow case where $\epsilon = 0$ is considered. This gives for the M, K, and S expressions

$$\begin{aligned}
M^0_{n,ac} &= \epsilon_n h L \delta_{a,c}, & K^0_{n,ac} &= \epsilon_n h L\left(\alpha_n^2 + \beta_a\beta_c\right)\delta_{a,c}, \\
M^1_{n,ac} &= \epsilon_n h L M_0 \delta_{a,c}, & K^1_{n,ac} &= \epsilon_n h L M_0\left(\alpha_n^2 + \beta_a\beta_c\right)\delta_{a,c}, \\
M^2_{n,ac} &= \epsilon_n h L M_0^2 \delta_{a,c}, & S_{n,ac} &= 0, \\
M^3_{n,ac} &= \epsilon_n h L M_0^3 \delta_{a,c}. &&
\end{aligned}$$

Using these expressions in the coefficients for the algebraic equations now gives

$$\begin{aligned}
X_0 = &\quad k^2M^0 - K^0 &&= \epsilon_n hL\delta_{a,c}\left[k^2 - \alpha_n^2 - \beta_a\beta_c\right], \\
X_1 = &\quad -3k^2M^1 + K^1 + 3S &&= \epsilon_n hL\delta_{a,c}\left[-3k^2M_0 + M_0\left(\alpha_n^2 + \beta_a\beta_c\right)\right], \\
X_2 = &\quad 3k^2M^2 - k^2M^0 &&= \epsilon_n hL\delta_{a,c}\left[3k^2M_0^2 - k^2\right], \\
X_3 = &\quad -k^2M^3 + k^2M^1 &&= \epsilon_n hL\delta_{a,c}\left[-k^2M_0^3 + k^2M_0\right].
\end{aligned}$$

Substituting these coefficients into the algebraic equation while assuming $a = c = m$ leads to

$$F(\lambda) = \left[k^2 - \alpha_n^2 - \beta_m^2\right] + \lambda\left[-3k^2M_0 + M_0\left(\alpha_n^2 + \beta_m^2\right)\right] + \lambda^2\left[3k^2M_0^2 - k^2\right] + \lambda^3\left[-k^2M_0^3 + k^2M_0\right] = 0.$$

Finally, this equation should be rewritten to see if it is similar to the derivation in Section 3.2 for the rectangular duct approximation with uniform flow.

$$\begin{aligned}
F(\lambda) &= -(\alpha_n^2 + \beta_m^2)[1 - \lambda M_0] - 3k^2M_0[1 - \lambda M_0]\lambda - k^2[1 - \lambda M_0]\lambda^2 + k^2 - k^2M_0^3\lambda^3 = 0 \\
&\implies F(\lambda) = (1 - \lambda M_0)\left[-\alpha_n^2 - \beta_m^2 - 3k^2M_0\lambda - k^2\lambda^2\right] \\
&\qquad + (k^2 - k^2M_0\lambda) + (k^2M_0\lambda - k^2M_0^2\lambda^2) + (k^2M_0^2\lambda^2 - k^2M_0^3\lambda^3) = 0 \\
&\implies F(\lambda) = (1 - \lambda M_0)\left[-\alpha_n^2 - \beta_m^2 - 3k^2M_0\lambda - k^2\lambda^2 + k^2 + k^2M_0\lambda + k^2M_0^2\lambda^2\right] = 0 \\
&\implies F(\lambda) = (1 - \lambda M_0)\left[k^2 - (\alpha_n^2 + \beta_m^2) - 2k^2M_0\lambda - k^2(1 - M_0^2)\lambda^2\right] = 0. \qquad (3.19)
\end{aligned}$$

Then solving $F(\lambda)$ for λ gives

$$\begin{aligned}
\lambda = \frac{1}{M_0} \quad \text{or} \quad \lambda &= \frac{2k^2M_0 \pm \sqrt{4k^4M_0^2 + 4k^2(1 - M_0^2)(k^2 - \alpha_n^2 - \beta^2)}}{-2(1 - \lambda M_0)k^2} \\
&= \frac{1}{1 - M_0^2}\left[-M_0 \pm \sqrt{1 - (1 - M_0^2)(\frac{\alpha_n^2 + \beta^2}{k^2})}\right],
\end{aligned}$$

and these solutions are similar to the ones derived in Section 3.2.

Chapter 4

Annular duct

4.1 Variational formulation

A sketch for the annular duct is repeated in Figure 4.1. The starting point for this derivation will be Pridmore-Brown's equation given as Equation (1) in [8]

$$\left(i\omega + w_0\frac{\partial}{\partial z}\right)\left[\frac{1}{c_0^2}\left(i\omega + w_0\frac{\partial}{\partial z}\right)^2 \hat{p} - \Delta\hat{p}\right] + 2\frac{\partial}{\partial z}(\nabla_\perp w_0 \cdot \nabla_\perp \hat{p}) = 0. \quad (4.1)$$

For the annular duct travelling wave solutions are sought of the form

$$\hat{p}(r,\theta,z) = q(r,\theta)e^{-ik\lambda z}.$$

Substitution of this expression into the Pridmore-Brown's equation leads to

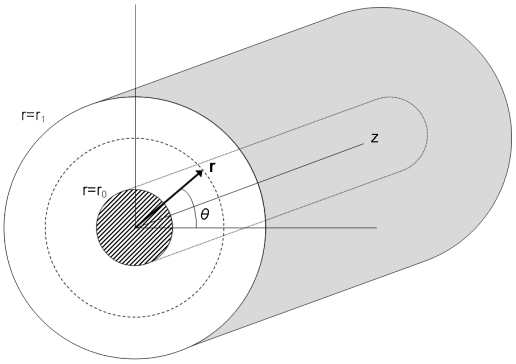

Figure 4.1: Fan plane of uniform annular duct model in cylindrical coordinates (r,θ,z).

$$(1-\lambda M_0)\left[\Delta_\perp q + k^2\left[(1-\lambda M_0)^2 - \lambda^2\right]q\right] + 2\lambda\left[\nabla_\perp M_0 \cdot \nabla_\perp q\right] = 0, \quad (4.2)$$

where $\nabla_\perp$ and $\Delta_\perp$ are the gradient operator and Laplacian, respectively, in the cross-section of the duct

$$\nabla_\perp = \left(\frac{\partial}{\partial r}, \frac{1}{r}\frac{\partial}{\partial \theta}\right) \quad \text{and} \quad \Delta_\perp = \frac{\partial^2}{\partial r^2} + \frac{1}{r}\frac{\partial}{\partial r} + \frac{1}{r^2}\frac{\partial^2}{\partial \theta^2}.$$

This equation is similar to Equation (3) in [8].

4.2 Dispersion relation

4.2.1 Uniform flow

For the uniform flow case $M_0(\theta) = \text{constant}$ ($\mathrm{d}M_0/\mathrm{d}\theta = 0$) and Equation (4.2) reduces to

$$(1-\lambda M_0)\left[\nabla_\perp q + k^2\left[(1-\lambda M_0)^2 - \lambda^2\right]q\right] = 0, \quad (4.3)$$

which has solutions

$$\lambda = \frac{1}{M_0} \quad \text{and} \quad \frac{\partial^2 q}{\partial r^2} + \frac{1}{r}\frac{\partial q}{\partial r} + \frac{1}{r^2}\frac{\partial^2 q}{\partial \theta^2} + k^2\left[(1-\lambda M_0)^2 - \lambda^2\right] = 0.$$

So, if solutions of the form

$$q_{mn} = A_{mn}Q_{mn}(r)e^{-im\theta},$$

are sought, then it can be seen that the term $Q_{mn}(r)$ is governed by the Bessel equation

$$\frac{\partial^2 Q_{mn}}{\partial r^2} + \frac{1}{r}\frac{\partial Q_{mn}}{\partial r} + \left(\kappa_{mn}^2 - \frac{m^2}{r^2}\right) Q_{mn} = 0, \tag{4.4}$$

and that the mode shapes are given by

$$Q_{mn}(r) = Y'_m(\kappa_{mn} h_r) J_m(\kappa_{mn} r) - J'_m(\kappa_{mn} h_r) Y_m(\kappa_{mn} r), \tag{4.5}$$

where $h_r = r_0/r_1$ is the hub-tip ratio which is equal to the (scaled) inner radius r_0. The radial wave numbers κ_{mn} are determined via boundary conditions $Q'_{mn}(1) = Q'_{mn}(h_r) = 0$ and are solutions of the characteristic equation [7]

$$Y'_m(z h_r) J'_m(z) - J'_m(z h_r) Y'_m(z) = 0, \tag{4.6}$$

where J_m and Y_m are the Bessel and Neumann functions of order m.
There are an infinite number of solutions corresponding to integer values of m and to the infinite number of values κ_{mn} defined by the eigenvalue equation, Equation (4.6). These modes of propagation are a combination of spinning modes and axial traveling waves. At a fixed z, angular traveling waves of the form

$$p \propto e^{(i(\omega t \pm m\theta))},$$

are observed, while at fixed z, angular traveling waves of the form

$$p \propto e^{(i(\omega t - k_z^{\pm} z))},$$

are observed. [6]
The axial wavenumber k_z is related to the radial wavenumber κ_{mn} through the dispersion relation in the duct

$$\begin{aligned} \kappa_{mn}^2 &= (k - M_0 k_z)^2 - k_z^2 \\ &\implies (1 - M_0) k_z^2 + 2k M_0 k_z + \kappa_{mn}^2 - k^2 = 0 \\ &\implies k_z = \frac{-k M_0}{1 - M_0^2} \pm \frac{\sqrt{k^2 - (1 - M_0^2)\kappa_{mn}^2}}{1 - M_0^2}. \end{aligned} \tag{4.7}$$

The axial wavenumber k_z can be real or complex depending on values of M_0 and κ_{mn}. k_z is real or cut-on if

$$(1 - M_0^2)\left(\frac{\kappa_{mn}}{k}\right)^2 < 1,$$

and complex or cut-off if

$$(1 - M_0^2)\left(\frac{\kappa_{mn}}{k}\right)^2 > 1.$$

In order to obtain the axial wave number k_z Equation (4.6) has to be used. The zeros of this equation provide the values of κ_{mn} (eigenvalues) and then by using the dispersion relation, Equation (4.7), the axial wave numbers k_z can be found.

4.2.2 Non-uniform flow

For the non-uniform flow case the following equation has to be solved

$$(1 - \lambda M_0)\left[\frac{\partial^2 q}{\partial r^2} + \frac{1}{r}\frac{\partial q}{\partial r} + \frac{1}{r^2}\frac{\partial^2 q}{\partial \theta^2} + k^2\left[(1 - \lambda M_0)^2 - \lambda^2\right] q\right] + 2\lambda\left[\frac{\partial M_0}{\partial \theta}\frac{\partial q}{\partial \theta}\right] = 0. \tag{4.8}$$

Substituting solutions of the form

$$q_{mn} = A_{mn} Q_{mn}(r) e^{-im\theta},$$

into Equation (4.8) now gives

$$(1 - \lambda M_0)\left[\frac{\partial^2 Q_{mn}}{\partial r^2} + \frac{1}{r}\frac{\partial Q_{mn}}{\partial r} - \frac{m^2}{r^2} Q_{mn} + k^2\left[(1 - \lambda M_0)^2 - \lambda^2\right] Q_{mn}\right] - 2i\lambda m \frac{\partial M_0}{\partial \theta} Q_{mn} = 0.$$

It follows that the term $Q_{mn}(r)$ is governed by the Bessel equation

$$\frac{\partial^2 Q_{mn}}{\partial r^2} + \frac{1}{r}\frac{\partial Q_{mn}}{\partial r} + \left(\kappa_{mn}^2 - \frac{m^2}{r^2}\right) Q_{mn} = 0, \tag{4.9}$$

where

$$\kappa_{mn}^2 = k^2\left[(1-\lambda M_0)^2 - \lambda^2\right] - \frac{2i\lambda m \frac{\partial M_0}{\partial \theta}}{1-\lambda M_0}.$$

In order to obtain the axial wavenumber k_z the following polynomial has to be solved

$$\left[M_0 - M_0^3\right] k_z^3 + \left[3kM_0^2 - k\right] k_z^2 + \left[\kappa_{mn}^2 M_0 - 3k^2 M_0 - 2im\frac{\partial M_0}{\partial \theta}\right] k_z + k^3 - k\kappa_{mn}^2 = 0. \tag{4.10}$$

4.3 Variational formulation

To derive the non-uniform flow case for the annular duct Pridmore-Brown's equation, Equation (4.1), is again recasted as a variational formulation

$$\int_A \left[(1-\lambda M_0)\left[k^2\overline{W}\left[(1-\lambda M_0)^2 - \lambda^2\right] q - \nabla_\perp \overline{W}\cdot\nabla_\perp q\right] + 3\lambda\overline{W}\nabla_\perp M_0\cdot\nabla_\perp q\right] \mathrm{d}A = 0, \tag{4.11}$$

where W is a trial function and A is the surface of the cross-section of the duct and solutions are sought of the form

$$\begin{aligned} q &= \sum A_{mn} Q_{mn}(r) e^{-im\theta} \\ &= \sum A_{mn} \underbrace{\psi_n(r)\phi_m(\theta)}_{W_{mn}}. \end{aligned}$$

M, K and S are defined exactly similar as in Section 3.3.2. For completeness these definitions and the expressions for the algebraic eigenvalue problem are repeated here.

$$M_{abcd}^{(s)} = \int_A M^s \overline{W}_{ab} W_{cd} \mathrm{d}A, \tag{4.12a}$$

$$K_{abcd}^{(s)} = \int_A M^s \nabla_\perp \overline{W}_{ab}\cdot\nabla_\perp W_{cd} \mathrm{d}A, \tag{4.12b}$$

$$S_{abcd} = \int_A \overline{W}_{ab}\nabla_\perp M\cdot\nabla_\perp W_{cd} \mathrm{d}A, \tag{4.12c}$$

for $s = 0, 1, 2, 3$. When these expressions are substituted into the variational statement, Equation (4.11), this leads to

$$\left(M^0 - 3\lambda M^1 + 3\lambda^2 M^2 - \lambda^3 M^3 - \lambda^2 M^0 + \lambda^3 M^1\right) k^2 + 3\lambda S - \left(K^0 - \lambda K^1\right) = 0,$$

and an algebraic eigenvalue problem for λ is obtained of the form

$$X_{abcd} A_{mn} = \left(X_0 + \lambda X_1 + \lambda^2 X_2 + \lambda^3 X_3\right) A_{mn} = 0, \tag{4.13}$$

where $X_0, ..., X_3$ are given by

$$\begin{aligned} X_0 &= k^2 M^0 - K^0, \\ X_1 &= -3k^2 M^1 + K^1 + 3S, \\ X_2 &= 3k^2 M^2 - k^2 M^0, \\ X_3 &= -k^2 M^3 + k^2 M^1. \end{aligned}$$

Furthermore, a flow distortion similar to the one defined in Section 3.3.1 is being considered for the

annular duct

$$\begin{aligned} M_0(\theta) &= M_0\left(1+\epsilon\cos\theta\right) \\ &= M_0\left(1+\frac{\epsilon}{2}\left(e^{i\theta}+e^{-i\theta}\right)\right), \\ \text{so } \frac{\mathrm{d}M_0}{d\theta} &= \frac{1}{2}i\epsilon M_0\left(e^{i\theta}-e^{-i\theta}\right). \end{aligned}$$

So, working out M^2 and M^3 leads to

$$\begin{aligned} M^2 &= M_0^2\left(1+2\epsilon\cos\theta+\epsilon^2\cos^2\theta\right) \\ &= M_0^2\left(1+\frac{\epsilon^2}{2}+2\epsilon\cos\theta+\frac{\epsilon^2}{2}\cos 2\theta\right), \\ M^3 &= M_0^3\left(1+\frac{\epsilon^2}{2}+2\epsilon\cos\theta+\frac{\epsilon^2}{2}\cos 2\theta\right)\left(1+\epsilon\cos\theta\right) \\ &= M_0^3\left(\left(1+\frac{\epsilon^2}{2}\right)+\left(3\epsilon+\frac{\epsilon^3}{2}\right)\cos\theta+2\epsilon^2\cos^2\beta_1 x+\frac{\epsilon^3}{2}\cos 2\theta\cos\theta+\frac{\epsilon^2}{2}\cos 2\theta\right) \\ &= M_0^3\left(\left(1+\frac{3\epsilon^2}{2}\right)+\left(3\epsilon+\frac{3\epsilon^3}{4}\right)\cos\theta+\frac{3\epsilon^2}{2}\cos 2\theta+\frac{\epsilon^3}{4}\cos 3\theta\right). \end{aligned}$$

Then, the following orthogonality relation is used in the derivation of the integrals from Equation (4.12) [9]

$$\int_0^{2\pi}\int_h^1 Q_{ab}(r)Q_{cd}(r)e^{ia\theta}e^{-ic\theta}r\mathrm{d}r\mathrm{d}\theta = 2\pi\delta_{ac}\delta_{bd}.$$

Working out the M, K and S integrals for $b=d=n$ is fixed and by using the obtained expressions for M^2 and M^3 and the orthogonality relation now gives

$$\begin{aligned} M^0_{n,ac} &= \int_A \overline{Q_{an}e^{-ia\theta}}Q_{cn}e^{-ic\theta}\mathrm{d}A \\ &= \int_0^{2\pi}\int_h^1 Q_{an}Q_{cn}e^{ia\theta}e^{-ic\theta}r\mathrm{d}r\mathrm{d}\theta = 2\pi\delta_{ac}\delta_{nn} = 2\pi\delta_{ac}, \\ M^1_{n,ac} &= \int_A \left[M_0+M_0\epsilon\cos\theta\right]Q_{an}e^{ia\theta}Q_{cn}e^{-ic\theta}\mathrm{d}A \\ &= M_0\int_0^{2\pi}\int_h^1\left[Q_{an}Q_{cn}e^{ia\theta}e^{-ic\theta}+\frac{\epsilon}{2}Q_{an}Q_{cn}e^{ia\theta}e^{-i(c-1)\theta}+\frac{\epsilon}{2}Q_{an}Q_{cn}e^{ia\theta}e^{-i(c+1)\theta}\right]r\mathrm{d}r\mathrm{d}\theta \\ &= \pi M_0\left[2\delta_{ac}+\epsilon\left(\delta_{a,c-1}+\delta_{a,c+1}\right)\int_h^1 Q_{an}Q_{cn}r\mathrm{d}r\right], \\ M^2_{n,ac} &= \int_A\left[M_0^2\left(1+\frac{\epsilon^2}{2}+2\epsilon\cos\theta+\frac{\epsilon^2}{2}\cos 2\theta\right)\right]Q_{an}e^{ia\theta}Q_{cn}e^{-ic\theta}\mathrm{d}A \\ &= \pi M_0^2\left[\left(2+\epsilon^2\right)\delta_{ac}+\epsilon\left(\frac{\epsilon}{2}\delta_{a,c-2}+2\delta_{a,c-1}+2\delta_{a,c+1}+\frac{\epsilon}{2}\delta_{a,c+2}\right)\int_h^1 Q_{an}Q_{cn}r\mathrm{d}r\right], \\ M^3_{n,ac} &= \int_A\left[M_0^3\left(\left(1+\frac{3\epsilon^2}{2}\right)+\left(3\epsilon+\frac{3\epsilon^3}{4}\right)\cos\theta+\frac{3\epsilon^2}{2}\cos 2\theta+\frac{\epsilon^3}{4}\cos 3\theta\right)\right]Q_{an}e^{ia\theta}Q_{cn}e^{-ic\theta}\mathrm{d}A \\ &= \pi M_0^3\left[\left(2+3\epsilon^2\right)\delta_{ac}+\left[\left(3\epsilon+\frac{3\epsilon^3}{4}\right)\left(\delta_{a,c-1}+\delta_{a,c+1}\right)+\frac{3\epsilon^2}{2}\left(\delta_{a,c-2}+\delta_{a,c+2}\right)\right.\right. \\ &\quad \left.\left.+\frac{\epsilon^3}{4}\left(\delta_{a,c-3}+\delta_{a,c+3}\right)\right]\int_h^1 Q_{an}Q_{cn}r\mathrm{d}r\right], \end{aligned}$$

$$
\begin{aligned}
K^0_{n,ac} &= \int_A \left[Q'_{an}Q'_{cn}e^{ia\theta}e^{-ic\theta} + Q_{an}Q_{cn}(ia)(-ic)e^{ia\theta}e^{-ic\theta}\right] \mathrm{d}A \\
&= 2\pi\delta_{ac}\left[ac + \int_h^1 Q'_{an}Q'_{cn}r\mathrm{d}r\right], \\
K^1_{n,ac} &= \int_A \left[M_0 + \epsilon M_0\cos\theta\right]\left[Q'_{an}Q'_{cn}e^{ia\theta}e^{-ic\theta} + Q_{an}Q_{cn}(ia)(-ic)e^{ia\theta}e^{-ic\theta}\right] \mathrm{d}A \\
&= 2\pi M_0\left[\delta_{ac}\left(ac + \int_h^1 Q'_{an}Q'_{cn}r\mathrm{d}r\right) + \epsilon\left(\delta_{a,c-1} + \delta_{a,c+1}\right)\left(\int_h^1 Q'_{an}Q'_{cn}r\mathrm{d}r + ac\int_h^1 Q_{an}Q_{cn}r\mathrm{d}r\right)\right], \\
S_{n,ac} &= \int_A Q_{an}e^{ia\theta}\left[\frac{1}{2}i\epsilon M_0\left(e^{i\theta} - e^{-i\theta}\right)\right](-ic)Q_{cn}e^{-ic\theta}\mathrm{d}A \\
&= \epsilon\pi c M_0\left(\delta_{a,c-1} - \delta_{a,c+1}\right)\int_h^1 Q_{an}Q_{cn}r\mathrm{d}r.
\end{aligned}
$$

It is decided to solve the integrals which contain product of solution Q numerically because it is expected that orthogonality does not hold for these cases.

4.3.1 Linearly approximated distortion

From the solution of the non-uniform flow case a solution for the linearly approximated distortion can be derived assuming that the distortion is linear in ϵ. This reduces the M, K and S integrals to

$$
\begin{aligned}
M^0_{n,ac} &= \int_A \overline{Q_{an}e^{-ia\theta}}Q_{cn}e^{-ic\theta}\mathrm{d}A \\
&= \int_0^{2\pi}\int_h^1 Q_{an}Q_{cn}e^{ia\theta}e^{-ic\theta}r\mathrm{d}r\mathrm{d}\theta = 2\pi\delta_{ac}\delta_{nn} = 2\pi\delta_{ac}, \\
M^1_{n,ac} &= \int_A \left[M_0 + M_0\epsilon\cos\theta\right]Q_{an}e^{ia\theta}Q_{cn}e^{-ic\theta}\mathrm{d}A \\
&= M_0\int_0^{2\pi}\int_h^1 \left[Q_{an}Q_{cn}e^{ia\theta}e^{-ic\theta} + \frac{\epsilon}{2}Q_{an}Q_{cn}e^{ia\theta}e^{-i(c-1)\theta} + \frac{\epsilon}{2}Q_{an}Q_{cn}e^{ia\theta}e^{-i(c+1)\theta}\right]r\mathrm{d}r\mathrm{d}\theta \\
&= \pi M_0\left[2\delta_{ac} + \epsilon\left(\delta_{a,c-1} + \delta_{a,c+1}\right)\int_h^1 Q_{an}Q_{cn}r\mathrm{d}r\right], \\
M^2_{n,ac} &= \int_A \left[M_0^2\left(1 + 2\epsilon\cos\theta\right)\right]Q_{an}e^{ia\theta}Q_{cn}e^{-ic\theta}\mathrm{d}A \\
&= \pi M_0^2\left[2\delta_{ac} + 2\epsilon\left(\delta_{a,c-1} + \delta_{a,c+1}\right)\int_h^1 Q_{an}Q_{cn}r\mathrm{d}r\right], \\
M^3_{n,ac} &= \int_A \left[M_0^3\left(1 + 3\epsilon\cos\theta+\right)\right]Q_{an}e^{ia\theta}Q_{cn}e^{-ic\theta}\mathrm{d}A \\
&= \pi M_0^3\left[2\delta_{ac} + 3\epsilon\left(\delta_{a,c-1} + \delta_{a,c+1}\right)\int_h^1 Q_{an}Q_{cn}r\mathrm{d}r\right], \\
K^0_{n,ac} &= \int_A \left[Q'_{an}Q'_{cn}e^{ia\theta}e^{-ic\theta} + Q_{an}Q_{cn}(ia)(-ic)e^{ia\theta}e^{-ic\theta}\right] \mathrm{d}A \\
&= 2\pi\delta_{ac}\left[ac + \int_h^1 Q'_{an}Q'_{cn}r\mathrm{d}r\right], \\
K^1_{n,ac} &= \int_A \left[M_0 + \epsilon M_0\cos\theta\right]\left[Q'_{an}Q'_{cn}e^{ia\theta}e^{-ic\theta} + Q_{an}Q_{cn}(ia)(-ic)e^{ia\theta}e^{-ic\theta}\right] \mathrm{d}A \\
&= 2\pi M_0\left[\delta_{ac}\left(ac + \int_h^1 Q'_{an}Q'_{cn}r\mathrm{d}r\right) + \epsilon\left(\delta_{a,c-1} + \delta_{a,c+1}\right)\left(\int_h^1 Q'_{an}Q'_{cn}r\mathrm{d}r + ac\int_h^1 Q_{an}Q_{cn}r\mathrm{d}r\right)\right], \\
S_{n,ac} &= \int_A Q_{an}e^{ia\theta}\left[\frac{1}{2}i\epsilon M_0\left(e^{i\theta} - e^{-i\theta}\right)\right](-ic)Q_{cn}e^{-ic\theta}\mathrm{d}A \\
&= \epsilon\pi c M_0\left(\delta_{a,c-1} - \delta_{a,c+1}\right)\int_h^1 Q_{an}Q_{cn}r\mathrm{d}r.
\end{aligned}
$$

4.3.2 Uniform flow

The solution for the uniform flow is obtained through simplifying the solution even further by taking $\epsilon = 0$, so

$$\begin{aligned}
M^0_{n,ac} &= \int_A \overline{Q_{an}e^{-ia\theta}}Q_{cn}e^{-ic\theta}\mathrm{d}A \\
&= \int_0^{2\pi}\int_h^1 Q_{an}Q_{cn}e^{ia\theta}e^{-ic\theta}r\mathrm{d}r\mathrm{d}\theta = 2\pi\delta_{ac}\delta_{nn} = 2\pi\delta_{ac}, \\
M^1_{n,ac} &= \int_A M_0 Q_{an}e^{ia\theta}Q_{cn}e^{-ic\theta}\mathrm{d}A \\
&= 2\pi M_0\delta_{ac}, \\
M^2_{n,ac} &= \int_A M_0^2 Q_{an}e^{ia\theta}Q_{cn}e^{-ic\theta}\mathrm{d}A \\
&= 2\pi M_0^2\delta_{ac}, \\
M^3_{n,ac} &= \int_A M_0^3 Q_{an}e^{ia\theta}Q_{cn}e^{-ic\theta}\mathrm{d}A \\
&= 2\pi M_0^3\delta_{ac}, \\
K^0_{n,ac} &= \int_A \left[Q'_{an}Q'_{cn}e^{ia\theta}e^{-ic\theta} + Q_{an}Q_{cn}(ia)(-ic)e^{ia\theta}e^{-ic\theta}\right]\mathrm{d}A \\
&= 2\pi\delta_{ac}\left[ac + \int_h^1 Q'_{an}Q'_{cn}r\mathrm{d}r\right], \\
K^1_{n,ac} &= \int_A M_0\left[Q'_{an}Q'_{cn}e^{ia\theta}e^{-ic\theta} + Q_{an}Q_{cn}(ia)(-ic)e^{ia\theta}e^{-ic\theta}\right]\mathrm{d}A \\
&= 2\pi M_0\delta_{ac}\left(ac + \int_h^1 Q'_{an}Q'_{cn}r\mathrm{d}r\right), \\
S_{n,ac} &= 0.
\end{aligned}$$

4.4 Normalization

In order to calculate the integrals containing Q numerically with MATLAB a suitable normalization has to be chosen. In [9] a normalization is proposed in such a way that

$$Q_{mn}(r) = N_{mn}\left(\cos(\tau_{mn})J_m(\kappa_{mn}r) - \sin(\tau_{mn})Y_m(\kappa_{mn}r)\right). \tag{4.14}$$

Now, if the normalization is chosen such that

$$\int_{h_r}^1 Q^2(r)rdr = 1, \tag{4.15}$$

then coefficients N_{mn} and τ_{mn} should be defined as

$$N_{mn} = \frac{\frac{1}{2}\sqrt{2}\pi\kappa_{mn}}{\left\{\frac{1-m^2/\kappa^2_{mn}}{J'_m(\kappa_{mn})^2+Y'_m(\kappa_{mn})^2} - \frac{1-m^2/\kappa^2_{mn}h_r^2}{J'_m(\kappa_{mn}h_r)^2+Y'_m(\kappa_{mn}h_r)^2}\right\}^{\frac{1}{2}}} \quad \text{and} \quad \tau_{mn} = \arctan\left\{\frac{J'_m(\kappa_{mn})}{Y'_m(\kappa_{mn})}\right\}.$$

Chapter 5

Results rectangular duct

5.1 Direct solver

For the rectangular duct geometry the problem was simply reduced to a set of independent equations of the form $X_{abcd}A_{mn} = 0$, where $X_{abcd} = X_0 + \lambda X_1 + \lambda^2 X_2 + \lambda^3 X_3$ (see Section 3.3). This can be solved as a linear eigenvalue problem $(X - \lambda B)A = 0$ with X, B and A defined as

$$\left[\begin{bmatrix} X_2 & X_0 & X_1 \\ 0 & 0 & I \\ I & 0 & 0 \end{bmatrix} - \lambda \begin{bmatrix} -X_3 & 0 & 0 \\ 0 & I & 0 \\ 0 & 0 & I \end{bmatrix}\right] \begin{bmatrix} \lambda^2 A \\ A \\ \lambda A \end{bmatrix} = \begin{pmatrix} 0 \\ 0 \\ 0 \end{pmatrix}. \tag{5.1}$$

The eigenvalues λ can be found using a direct solver MATLAB routine which calculates $\det(X - \lambda B) = 0$. This should result in a set of three different eigenvalues and eigenvectors for each mode (m, n). The eigenvalues should correspond to one hydrodynamic mode and two acoustic modes of which one matches with the positive direction of propagation and the other with the negative direction. Here the positive acoustic modes correspond to downstream propagation and the negative acoustic modes correspond to upstream propagation. The eigenvectors can be reduced to three scalar values of the amplitude A_{mn}, because the first and third component are just multiples of λ.

In the uniform flow case a matrix of size $m \times m$ has to be solved for every radial mode order n. This matrix will only have polynomials X_{ac} on the diagonal while the remaining matrix will be empty. However, for the linear and nonlinear approximation of the non-uniform flow terms will appear on either side of the diagonal, where every single term is a cubic equation.

To give an idea where this leads to, the total matrix in is given for the linearly approximated flow case with three circumferential modes m and radial mode order n

$$\begin{bmatrix} X_{n,a-1,c-2} & X_{n,a-1,c} & X_{n,a-1,c+1} & 0 & 0 \\ 0 & X_{n,a,c-1} & X_{n,a,c} & X_{n,a,c+1} & 0 \\ 0 & 0 & X_{n,a+1,c} & X_{n,a+1,c+1} & X_{n,a+1,c+2} \end{bmatrix} \begin{bmatrix} A_{n,a-2,c-2} \\ A_{n,a-1,c-1} \\ A_{n,a,c} \\ A_{n,a+1,c+1} \\ n, A_{a+2,c+2} \end{bmatrix} = 0,$$

where every X-term is a cubic equation. Note that the row values of the different m-modes are given by integers a and that the column values are given by integers c. In order to obtain a square matrix the red values are left out. So, solving this system leads to nine different eigenvalues and three different amplitudes for mode (m, n), where $A_{n,a-1,c-1}$ and $A_{n,a+1,c+1}$ are the contributions from modes $(m-1, n)$ and $(m+1, n)$ into mode (m, n). From this definition of the matrix it should be noted that the solutions at the boundary values of m are less accurate because the matrix is assumed to be square.

5.1.1 MATLAB code

The MATLAB code for the non-uniform flow in the rectangular approximation for the annular duct consists of few calculating and sorting steps. Therefore, a concise summary of the different steps in the

code is given in the flowchart of Figure 5.1. The eigenvalues and eigenvectors are calculated by using the built-in function 'eig' in MATLAB which uses the QZ or generalized Schur algorithm to solve the generalized eigenvalue problem for square matrices X and B.

Sorting the eigenvalues into hydrodynamic and positive or negative acoustic modes is an important part of the MATLAB code. Some expressions which are derived in Section 3.2 can be used in this case. Firstly, when the obtained eigenvalue has a nonzero imaginary part, it should be categorized as a positive acoustic mode if $\Im(\lambda) < 0$ and as a negative acoustic mode if $\Im(\lambda) > 0$. Furthermore, the shift between the zero-imaginary axis and the real imaginary values is equal to $M_0/(M_0^2 - 1)$. Thus, if

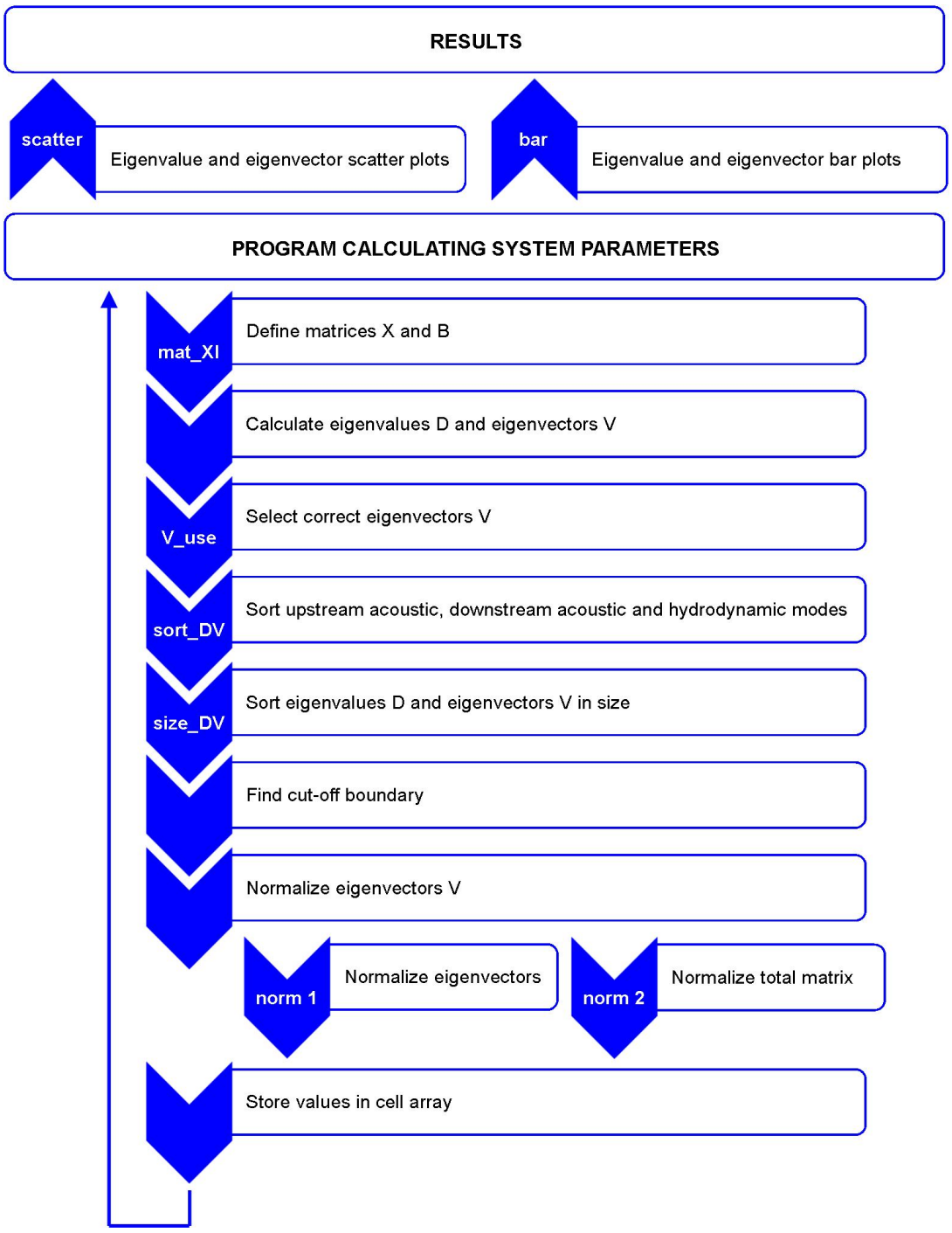

Figure 5.1: Flowchart of MATLAB code.

the mode value has a zero imaginary part, it should be categorized as an negative acoustic mode if its value is smaller than $M_0/(M_0^2-1)$ and as a positive acoustic mode if otherwise. Finally, the only issue remaining is the distinction between real positive acoustic modes and hydrodynamic modes. This can be done by assuming that the hydrodynamic modes should be near $1/M_0$ and that the acoustic modes approximately stay between the outer boundary values determined by

$$\lambda = \frac{M_0 \pm 1}{M_0^2 - 1}. \tag{5.2}$$

Finally, there are two different kind of normalizations implemented in the code. Normalization 1 normalizes every single eigenvector to its maximum value while normalization 2 normalizes all the eigenvectors in the total solved system to the maximum value occurring in that particular system.

The MATLAB code for calculating the system parameters and for plotting the results (upper three rows of the flowchart in Figure 5.1) for a system with linear flow distortion in a rectangular duct is included in Appendix B.

5.2 Validation

To validate the MATLAB code for solving the generalized linear eigenvalue problem $(X - \lambda B)A = 0$ a comparison is made with the eigenvalues obtained from the Newton-Raphson method in Section 3.2. A rather low Helmholtz number ($H_n = 10$) is chosen to keep the results surveyable. The other constants are set to

$$M_0 = 0.4; \quad H_n = kh = 10; \quad r_1 = 1.3 \text{ m}; \quad r_0 = 0.3 \text{ m}; \quad h = r_1 - r_0 = 1 \text{ m}.$$

In Figure 5.2 the eigenvalues are plotted for the first six $n-$modes and $m-$modes ranging from -1 to 1. The results obtained by using the direct solver for $\epsilon = 0$ are given in Figure 5.3. It can be seen that the values are similar to the ones in Figure 5.2. The value of the hydrodynamic modes is 2.5 which is to be expected since $\lambda = 1/M_0 = 2.5$.

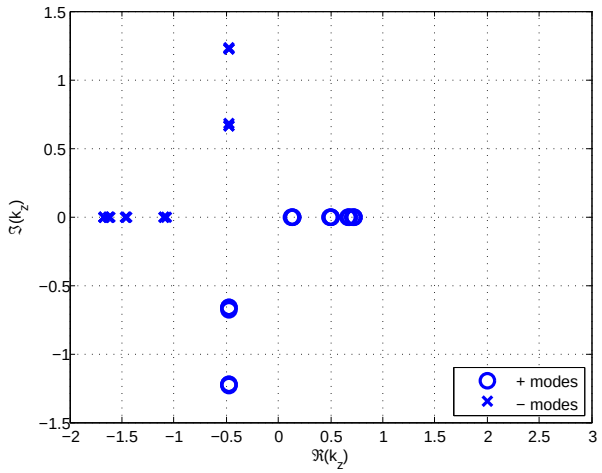

Figure 5.2: Eigenvalues for the uniform flow case with $m = [-1, 1], n = [1, 6], M_0 = 0.4, H_n = kh = 10, h = 1$.

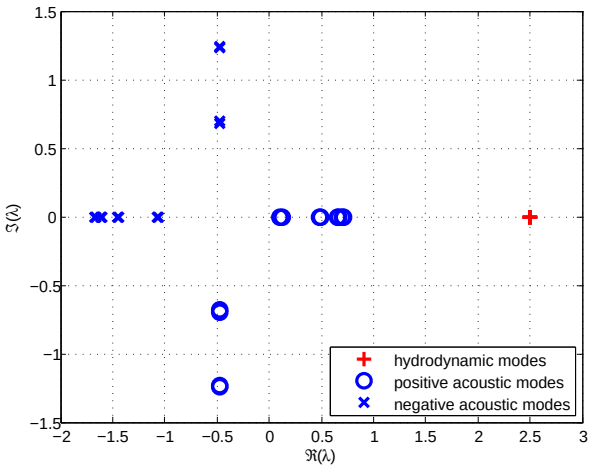

Figure 5.3: Eigenvalues for $\epsilon = 0$ using the direct method and $m = [-1, 1], n = [1, 6], M_0 = 0.4, H_n = kh = 10, h = 1$.

5.3 Results

In engine acoustics the higher mode orders are physically more interesting. Therefore, results for a system around circumferential mode order $m = 24$ are shown in this section. Furthermore, it is assumed that a range of 10 modes around the central value $m = 24$ is enough to reflect all influences from the

neighbouring modes. The solver is able to calculate both downstream and upstream modal amplitudes. Since the latter are more interesting, they are shown in this section while the downstream solutions are included in Appendix A, Section A.1.
The Helmholtz number for the systems is chosen such that all modes $m = [14, 34]$ are cut-on when there is no distortion. Furthermore, the radial mode order n is set to 1.

5.3.1 Linear approximation

In Figure 5.4 the eigenvalue plots are shown for four different values of ϵ, $\epsilon = 0, 0.01, 0.05$ and 0.1. It can be seen that all modes remain cut-on for the first three values of distortion, while mode $m = 34$ is cut-off for $\epsilon = 0.1$. So, it can be concluded that flow distortion influences the cut-off ratio.

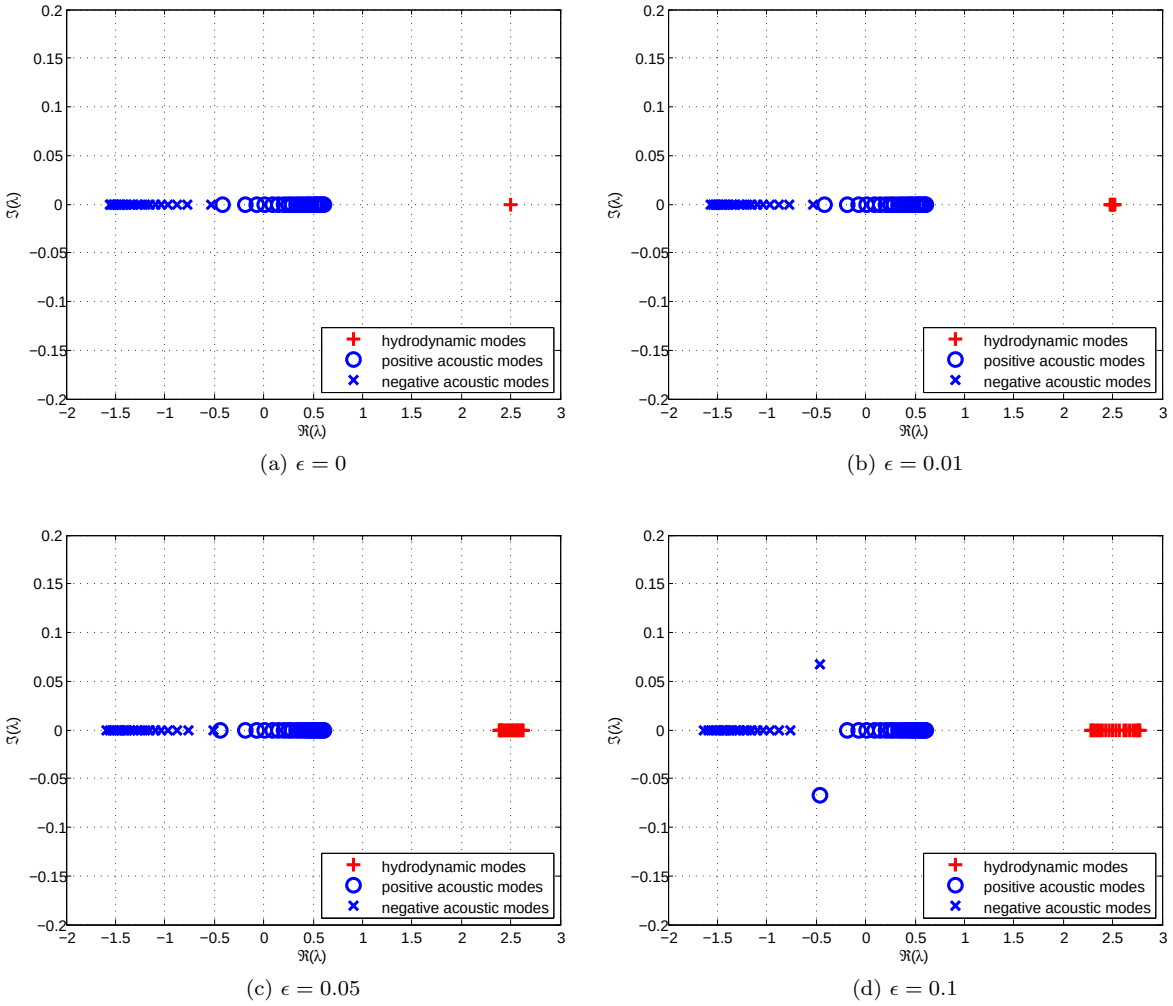

(a) $\epsilon = 0$ (b) $\epsilon = 0.01$

(c) $\epsilon = 0.05$ (d) $\epsilon = 0.1$

Figure 5.4: Eigenvalues for different values of ϵ assuming linear flow distortion and $m = [14, 34], n = 1, M_0 = 0.4, H_n = kh = 39, h = 1$.

The results for the modal amplitudes are given in Figure 5.5. The plots on the left are the amplitude solution for mode $m = 24$ only and this solution is normalized with the largest amplitudal value appearing in that solution (normalization 1). The plots on the right show the amplitudes for the whole system $m = [14, 34]$ and here the total system is normalized with the largest value existing in the total system (normalization 2). The plots on the left are just a vertical slice at mode $m = 24$ on the x-axis. It can be seen that, for lower flow distortion factors, the contribution from neighbouring modes increases with ϵ. However, at some point little below $\epsilon = 0.05$, the amplitudes of adjacent modes $m = 23$ and $m = 25$ become larger than the amplitude of mode $m = 24$. From the plots on the right in Figure 5.5 it can be

concluded that the amplitudes increase with circumferential mode order m.

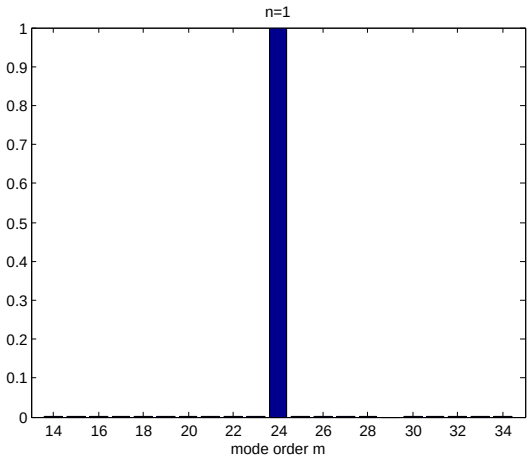

(a) Mode m=24, $\epsilon = 0$

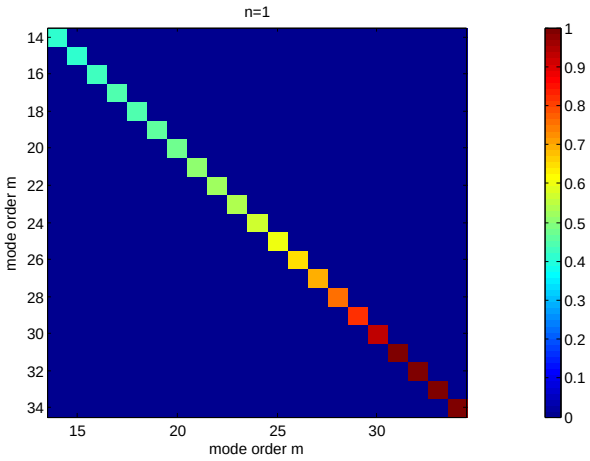

(b) Total system, $\epsilon = 0$

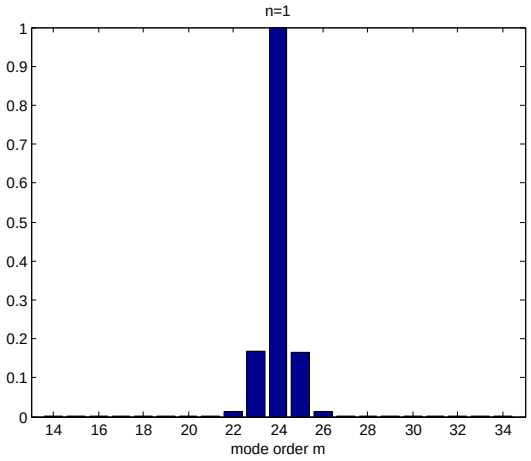

(c) Mode m=24, $\epsilon = 0.01$

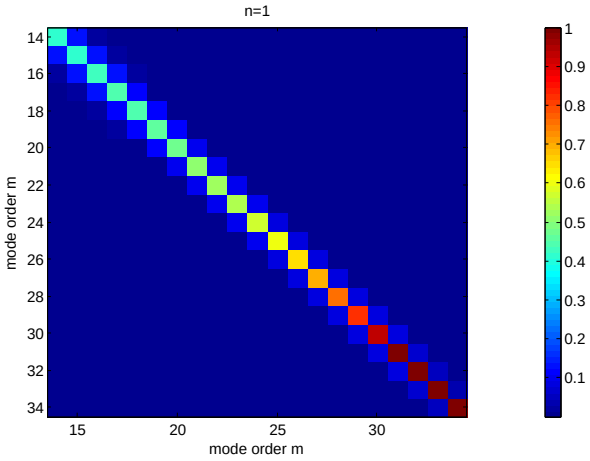

(d) Total system, $\epsilon = 0.01$

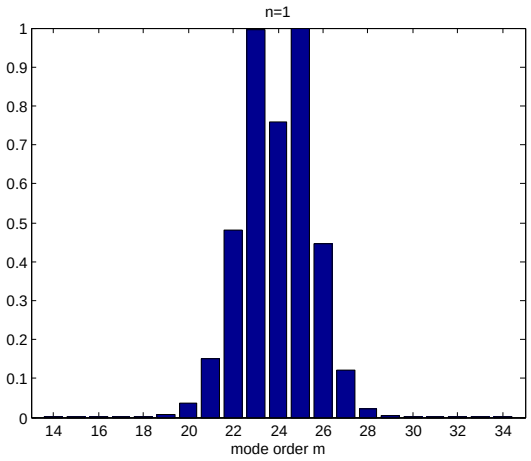

(e) Mode m=24, $\epsilon = 0.05$

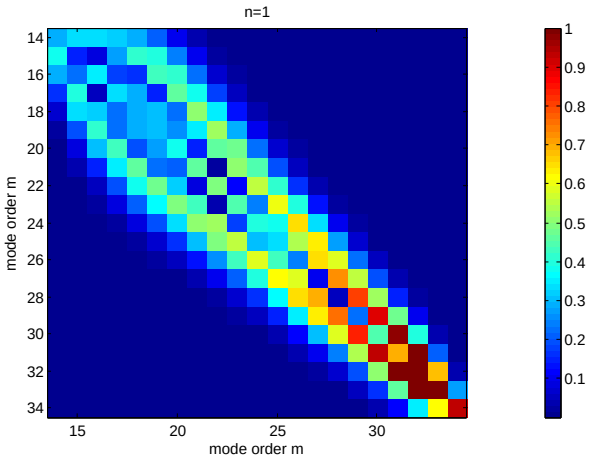

(f) Total system, $\epsilon = 0.05$

Figure 5.5: Modal amplitudes for different values of ϵ assuming linear flow distortion and $m = [14, 34], n = 1, M_0 = 0.4, H_n = kh = 39, h = 1$.

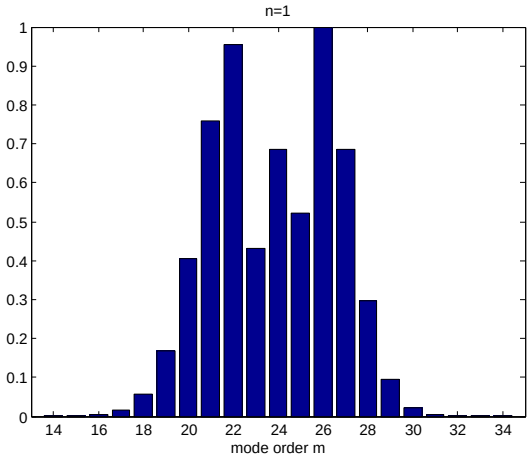

(g) Mode m=24, $\epsilon = 0.1$

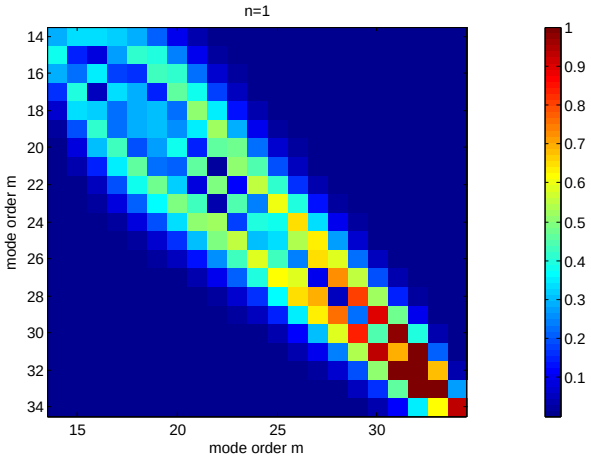

(h) Total system, $\epsilon = 0.1$

Figure 5.5: Modal amplitudes for different values of ϵ assuming linear flow distortion and $m = [14, 34], n = 1, M_0 = 0.4, H_n = kh = 39, h = 1$.

5.3.2 Nonlinear approximation

For the nonlinear approximation of the flow distortion the eigenvalue plots in Figure 5.6 look similar to the eigenvalue plots for the linear approximation in Figure 5.4 for the acoustic modes. The hydrodynamic modes for the nonlinear approximation stay in the same region, but their values become imaginary at some point.
The amplitude plots in Figure 5.7 for low distortion factors also look similar to the results for the linear approximation with the difference that the contributions from modes $m = 22$ and $m = 23$ are slightly larger in the nonlinear case. For higher values of ϵ, amplitudes of the nonlinear approximation are less symmetrically shaped than in the linear case.

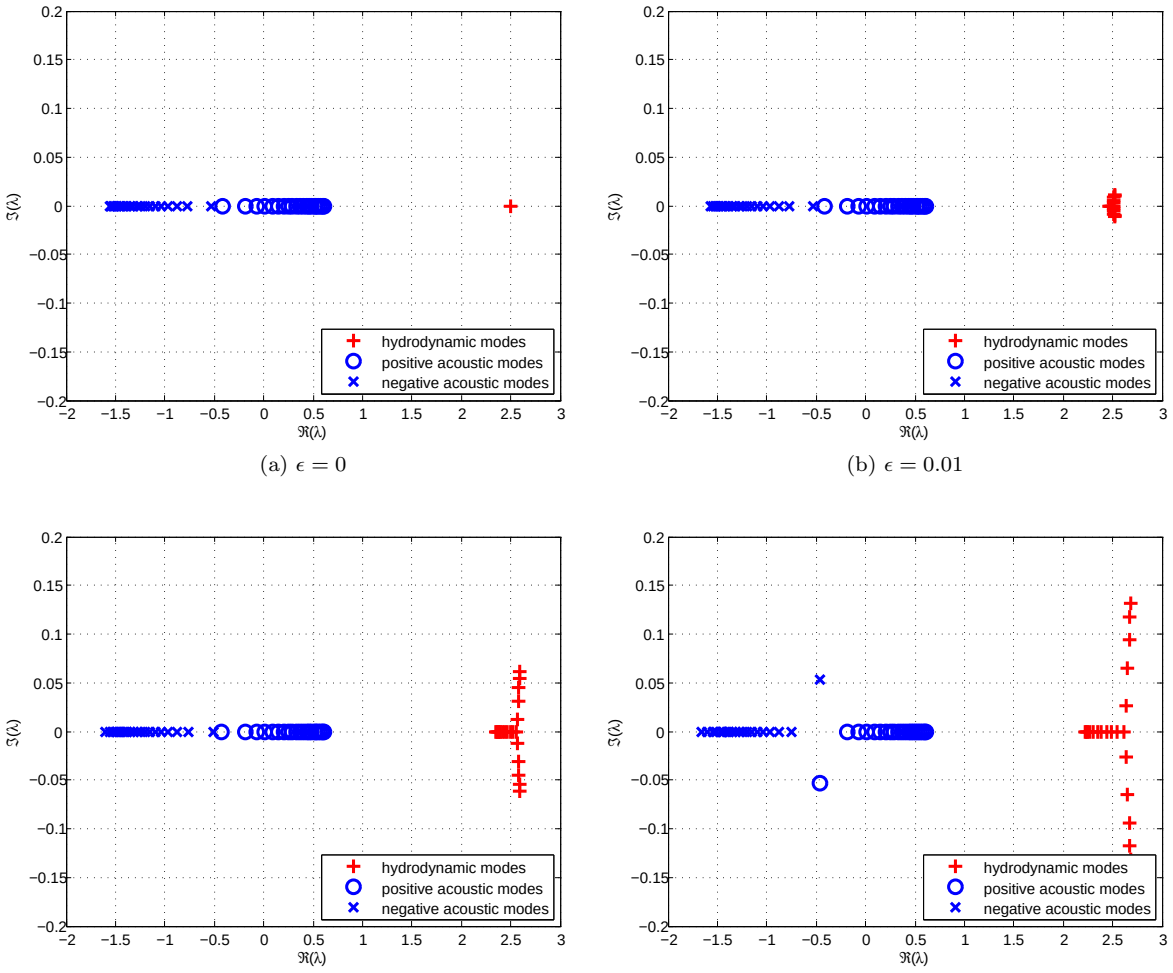

(a) $\epsilon = 0$ (b) $\epsilon = 0.01$

(c) $\epsilon = 0.05$ (d) $\epsilon = 0.1$

Figure 5.6: Eigenvalues for different values of ϵ assuming nonlinear flow distortion and $m = [14, 34], n = 1, M_0 = 0.4, H_n = kh = 39, h = 1$.

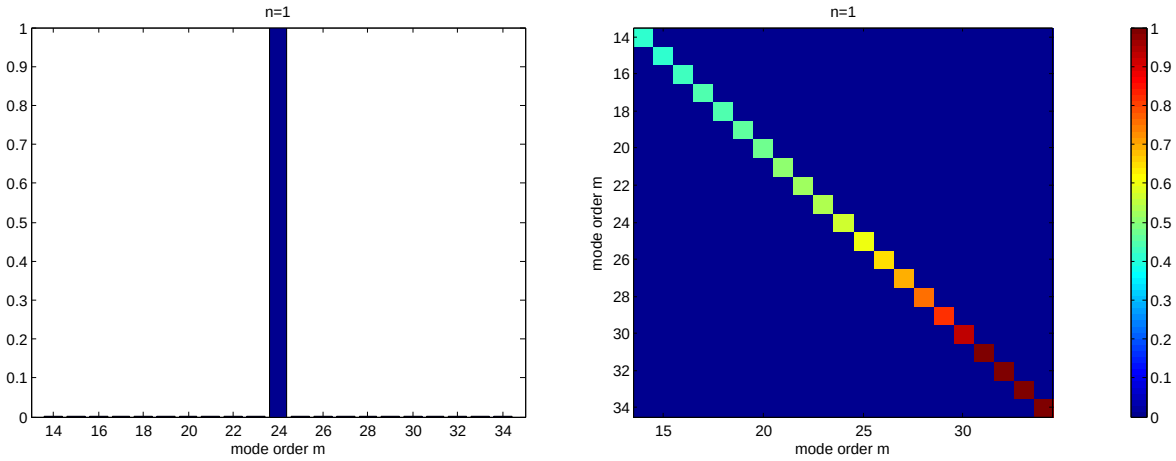

(a) Mode m=24, $\epsilon = 0$ (b) Total system, $\epsilon = 0$

Figure 5.7: Modal amplitudes for different values of ϵ assuming nonlinear flow distortion and $m = [14, 34], n = 1, M_0 = 0.4, H_n = kh = 39, h = 1$.

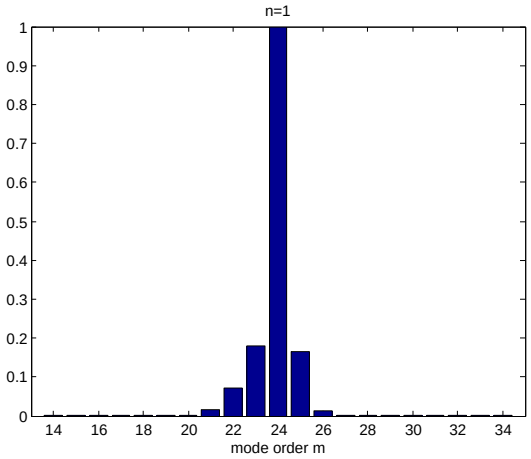

(c) Mode m=24, $\epsilon = 0.01$

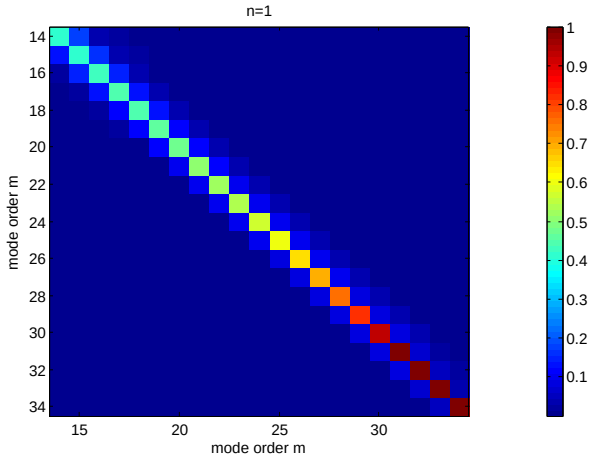

(d) Total system, $\epsilon = 0.01$

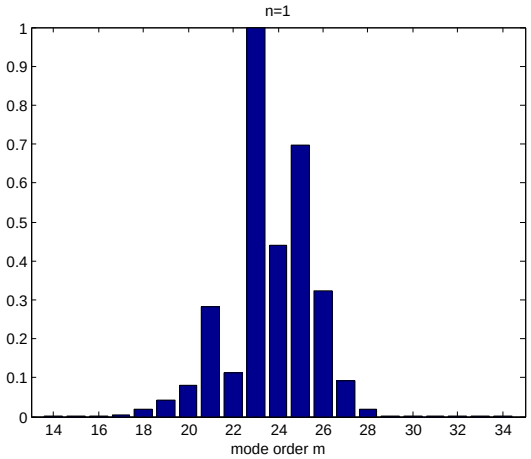

(e) Mode m=24, $\epsilon = 0.05$

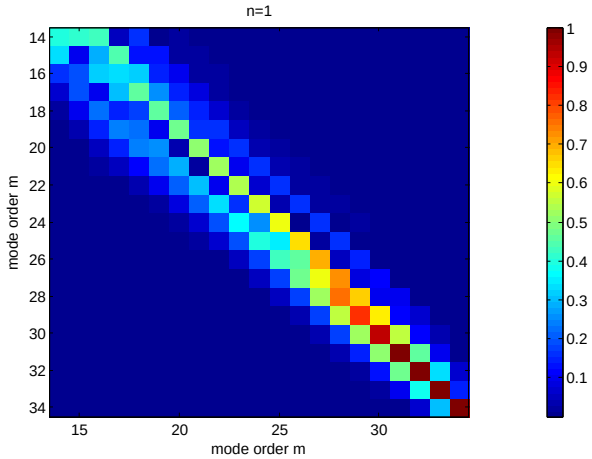

(f) Total system, $\epsilon = 0.05$

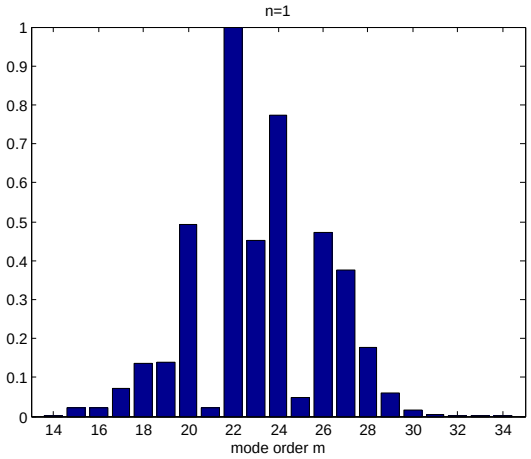

(g) Mode m=24, $\epsilon = 0.1$

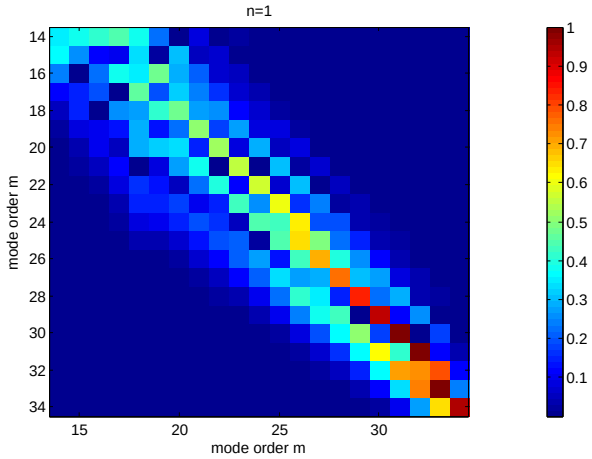

(h) Total system, $\epsilon = 0.1$

Figure 5.7: Modal amplitudes for different values of ϵ assuming nonlinear flow distortion and $m = [14, 34], n = 1, M_0 = 0.4, H_n = kh = 39, h = 1$.

Chapter 6

Rolls-Royce data

This chapter is removed because its content is regarded as strictly confidential to Rolls-Royce. The original version of this appendix is archived at the Rolls-Royce UTC in ISVR Southampton and is only accessible by its members.

Chapter 7

Conclusions and Future work

7.1 Conclusions

From the numerical results in Chapter 5 it can be concluded that flow distortion influences propagating modes and that this effect is larger if the distortion factor ϵ increases. At low values of ϵ (< 0.05) the results for the linear and nonlinear approximation of the flow distortion look almost similar. This is to be expected since the linear approximation is only a simplification of the nonlinear one. For larger values of ϵ however, the 'randomness' in the results for the nonlinear approximation seems to increase. Sometimes it seems that particular modal amplitudes are calculated incorrectly and therefore do not have a value as large as should be expected from comparison with the linear approximation.

7.2 Future work

This research marked the beginning on studying the effect of flow distortion on modes propagating in a turbofan intake duct and there is still a lot that can be done on the subject. First of all, it will be of great value to implement the annular duct model and to see if there are more and/or better similarities with the data from Rolls-Royce. The next step could then be to implement a liner in the annular duct and trying to solve it with, for instance, a Finite Element Method. The ultimate goal would be to develop some kind of prediction method for the effect of flow distortion in lined ducts.

Bibliography

[1] Institute of sound and vibration research, university of southampton. http://www.soton.ac.uk/engineering/research/centres/isvr.page, Feb. 2012.

[2] Rolls-royce plc. http://www.rolls-royce.com/, 2012.

[3] Achunche, I. M. Acoustic optimisation and prediction of sound propagation in turbofan engine ducts. EngD thesis, Institute of Sound and Vibration Research, Faculty of Engineering, Science and Mathematics, University of Southampton, Jan. 2010.

[4] Astley, R. J. *Propulsion System Noise: Turbomachinery*, vol. Encyclopedia of Aerospace Engineering. John Wiley & Sons, Ltd, 2010.

[5] Brooks, C. J. Prediction and control of sound propagation in turbofan engine bypass ducts. EngD thesis, Institute of Sound and Vibration Research, Faculty of Engineering, Science and Mathematics, University of Southampton, Sept. 2007.

[6] Eversman, W. *Aeroacoustics of Flight Vehicles: Theory and Practice*, vol. 2: Noise Control, Chapter 13: Theoretical Models for Duct Acoustic Propagation and Radiation. NASA Office of Management, Scientific and Technical Information Program, 1991.

[7] Gabard, G., and Astley, R. J. Theoretical model for sound radiation from annular jet pipes: far- and near-field solutions. *Journal of Fluid Mechanics 549* (2006), 315–341.

[8] Gabard, G., and Astley, R. J. A computational mode-matching approach for sound propagation in three-dimensional ducts with flow. *Journal of Sound and Vibration 315*, 4 (Mar. 2008), 1103–1124.

[9] Rienstra, S. W., and Hirschberg, A. An introduction to acoustics. Eindhoven University of Technology, extended and revised edition of IWDE 92-06, http://www.win.tue.nl/~sjoerdr/papers/boek.pdf, Jan. 2012.

Appendix A

Numerical results

A.1 Results downstream acoustic modes in rectangular duct

A.1.1 Linear approximation

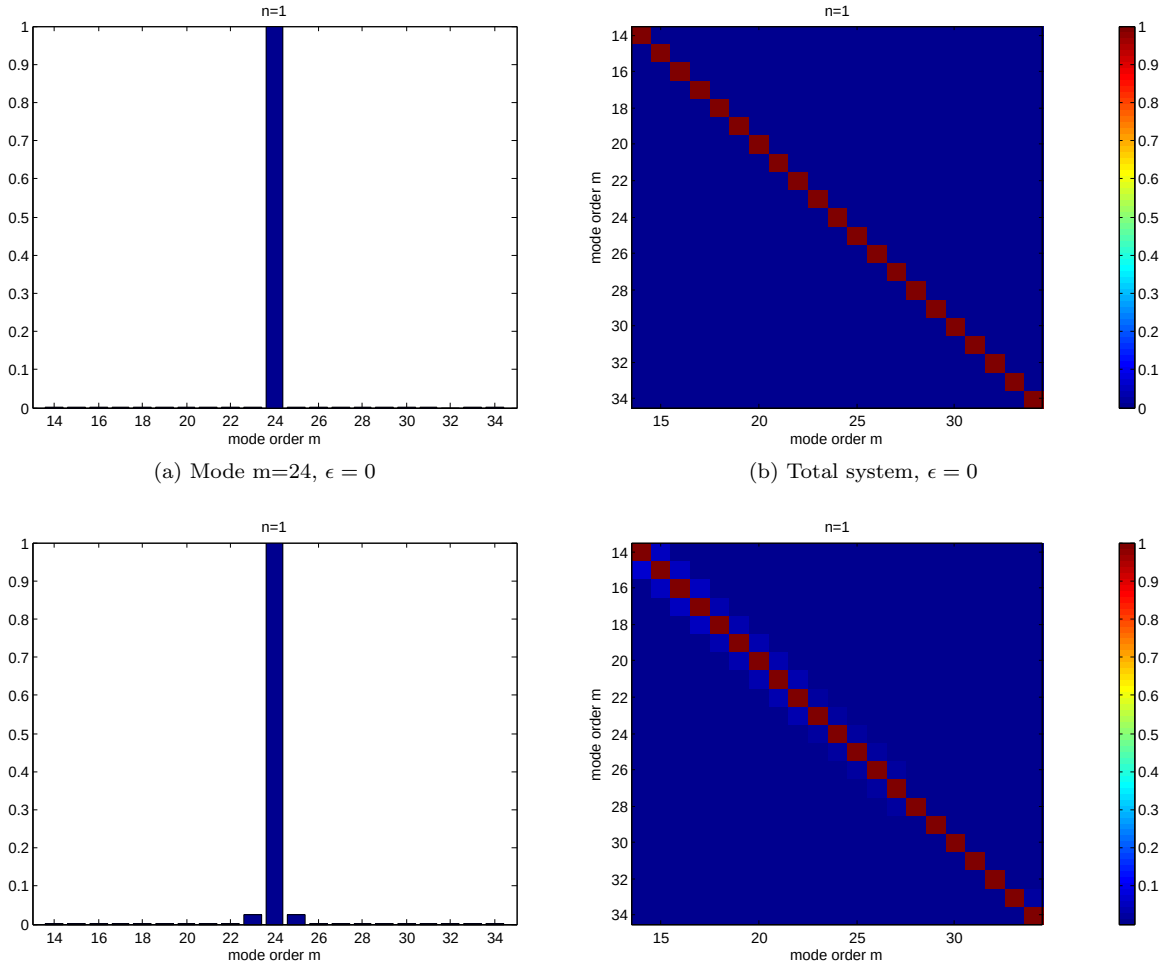

(a) Mode m=24, $\epsilon = 0$

(b) Total system, $\epsilon = 0$

(c) Mode m=24, $\epsilon = 0.01$

(d) Total system, $\epsilon = 0.01$

Figure A.1: Modal amplitudes (downstream) for different values of ϵ assuming linear flow distortion and $m = [14, 34], n = 1, M_0 = 0.4, H_n = kh = 39, h = 1$.

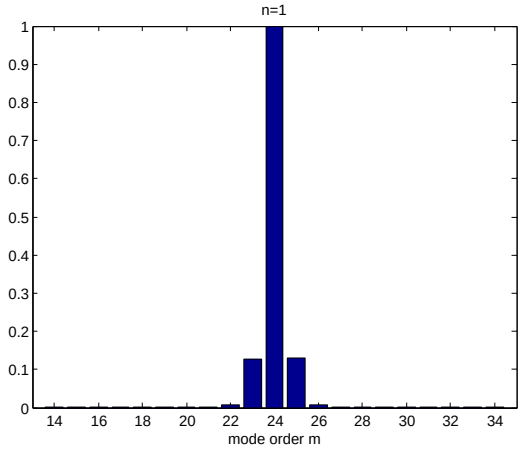

(e) Mode m=24, $\epsilon = 0.05$

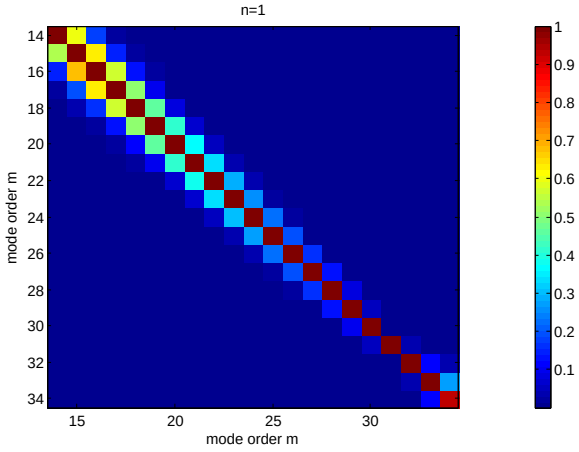

(f) Total system, $\epsilon = 0.05$

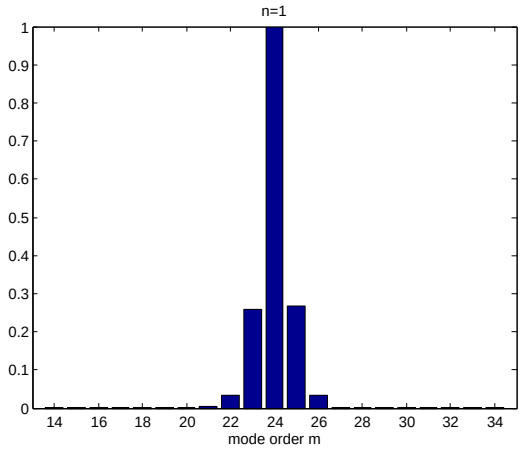

(g) Mode m=24, $\epsilon = 0.1$

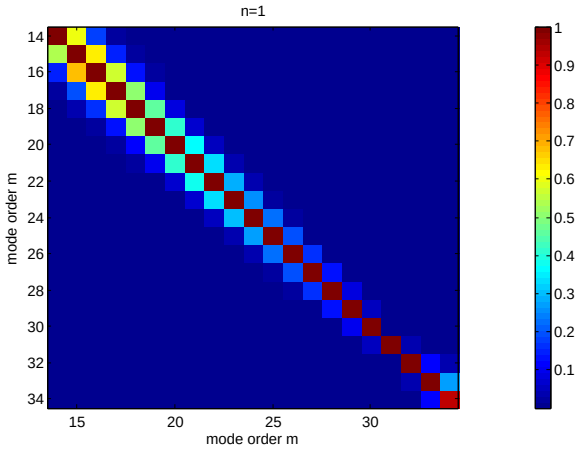

(h) Total system, $\epsilon = 0.1$

Figure A.1: Modal amplitudes (downstream) for different values of ϵ assuming linear flow distortion and $m = [14, 34], n = 1, M_0 = 0.4, H_n = kh = 39, h = 1$.

A.1.2 Nonlinear approximation

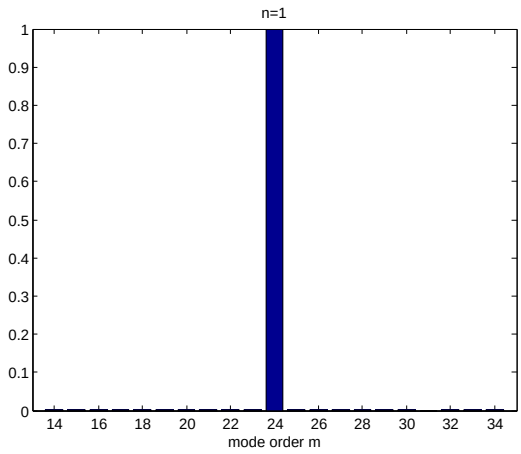

(a) Mode m=24, $\epsilon = 0$

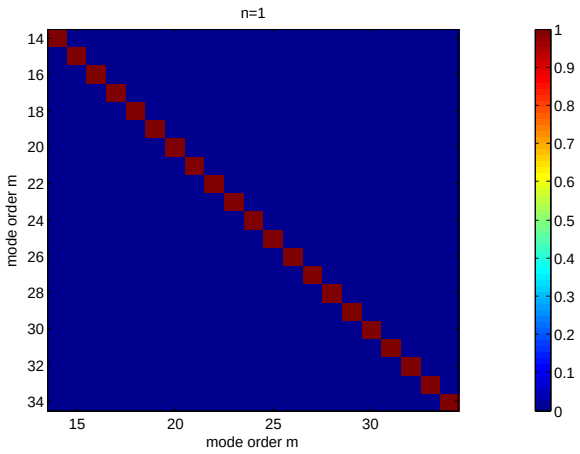

(b) Total system, $\epsilon = 0$

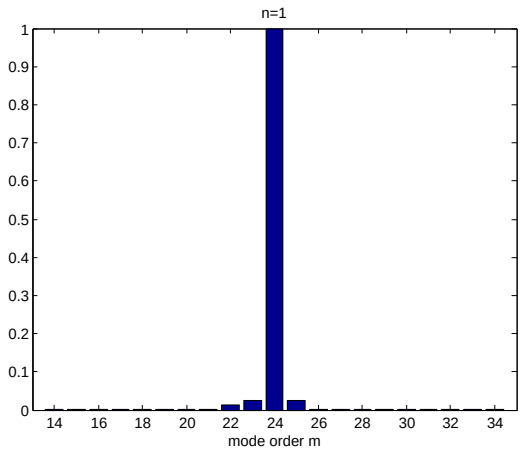

(c) Mode m=24, $\epsilon = 0.01$

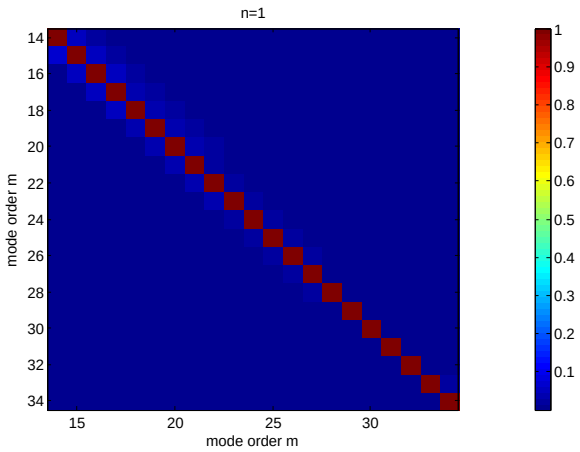

(d) Total system, $\epsilon = 0.01$

Figure A.2: Modal amplitudes (downstream) for different values of ϵ assuming nonlinear flow distortion and $m = [14, 34], n = 1, M_0 = 0.4, H_n = kh = 39, h = 1$.

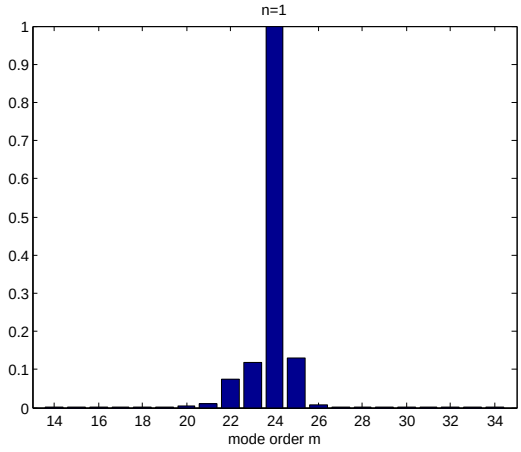

(e) Mode m=24, $\epsilon = 0.05$

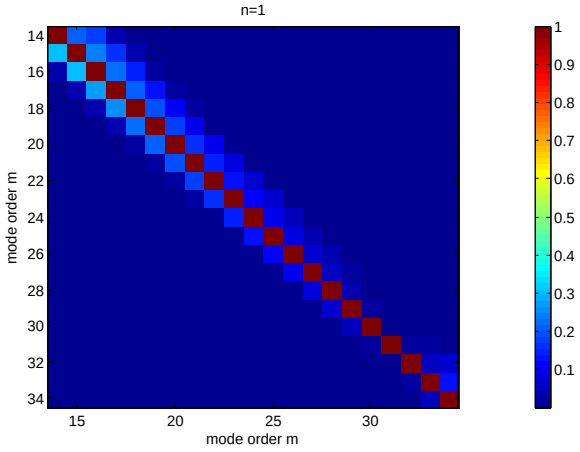

(f) Total system, $\epsilon = 0.05$

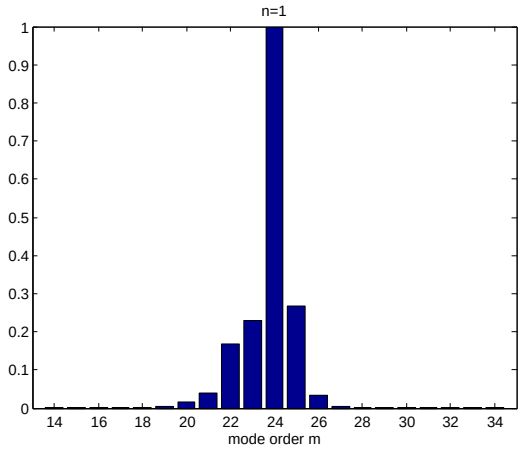

(g) Mode m=24, $\epsilon = 0.1$

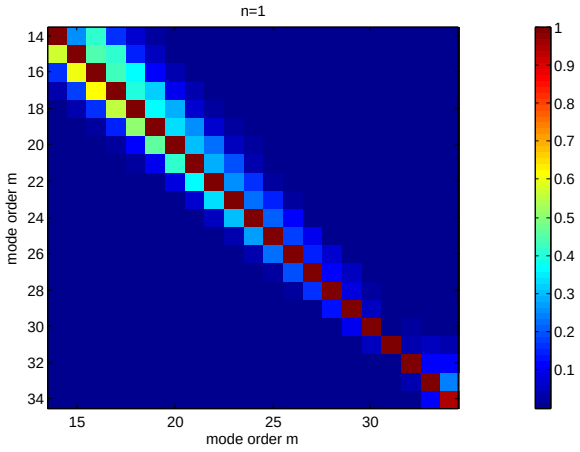

(h) Total system, $\epsilon = 0.1$

Figure A.2: Modal amplitudes (downstream) for different values of ϵ assuming nonlinear flow distortion and $m = [14, 34], n = 1, M_0 = 0.4, H_n = kh = 39, h = 1$.

Appendix B

MATLAB code

The following three MATLAB m-files are included in this appendix

rect_linear.m	code calculating system parameters for a rectangular duct with linear flow distortion,
rect_linear_plot.m	code producing results in scatter plots,
rect_linear_plotbar.m	code producing results in bar plots.

```
function [XC,IC,DC,D_NEG,D_POS,D_HYD,VC,V_NEG,V_POS,V_HYD,CO_NEG,CO_POS]...
    = rect_linear(n,mmin,mmax,epsi,norm)
%=========================================================================
% RECT_LINEAR(n,mmin,mmax,epsi): calculates matrices X and I, eigenvalues D
% and eigenvectors V for a two-dimensional rectangular duct with a linear
% flow distortion. The eigenvalues and eigenvectors are categorized as
% hydrodynamic and acoustic values and ordered and normalized as well.
%
% INPUT
% n:        radial mode order n
% mmin:     lower bound circumferential mode order m
% mmax:     upper bound circumferential mode order m
% epsi:     flow distortion factor
% norm:     normalization 1 - normalizes individual eigenvectors
%           normalization 2 - normalizes all eigenvectors together
%
% OUTPUT
% XC:       cell-array matrix X
% IC:       cell-array matrix I
% DC:       cell-array eigenvalues
% D_NEG:    cell-array negative acoustic eigenvalues (upstream)
% D_POS:    cell-array positive acoustic eigenvalues (downstream)
% D_HYD:    cell-array hydrodynamic eigenvalues
% VC:       cell-array eigenvectors
% V_NEG:    cell-array negative acoustic eigenvectors (upstream)
% V_POS:    cell-array positive acoustic eigenvectors (downstream)
% V_HYD:    cell-array hydrodynamic eigenvectors
% CO_NEG:   cell-array first negative cut-off mode order m (upstream)
% CO_POS:   cell-array first positive cut-off mode order m (downstream)
%=========================================================================

% Determine position central mode
MM = ((mmax-mmin)/2)+1;

% Complete loop for every value of n
for ii=1:n
    % Define matrices
    [X,I] = mat_XI(ii,mmin,mmax,epsi);

    % Calculate eigenvalues A = [X-\lambdaI]
    [V,D] = eig(X,I,'qz');

    % Select correct amplitudes
    [V] = V_use(V);

    % Sort eigenvalues and eigenvectors in categories
    [D_hyd,D_neg,D_pos,V_hyd,V_neg,V_pos] = sort_DV(D,V);

    % Sort eigenvalues and eigenvectors of acoustic modes in size
    [D_neg,D_pos,V_neg,V_pos] = size_DV(D_neg,D_pos,V_neg,V_pos);

    % Find cut-off boundary
    if n<=9

        for jj=1:length(V_neg)
            RE = isreal(V_neg(:,jj));
            if RE == 0
                CO_neg = jj;
                break
            end
        end
        for jj=1:length(V_pos)
            RE = isreal(V_pos(:,jj));
```

```
            if RE == 0
                CO_pos = jj;
                break
            end
        end

    elseif n>9 && ii==n

        for jj=1:length(V_neg)
            RE = isreal(V_neg(:,jj));
            if RE == 0
                CO_neg = jj;
                break
            end
        end
        for jj=1:length(V_pos)
            RE = isreal(V_pos(:,jj));
            if RE == 0
                CO_pos = jj;
                break
            end
        end

    else
        CO_neg = [];
        CO_pos = [];
    end

    % Normalization
    if norm==1
        % Normalize eigenvectors
        [V_neg,V_pos] = norm_V(V_neg,V_pos);
    elseif norm==2
        % Normalization total matrix
        Vn_neg = abs(V_neg);
        Vn_pos = abs(V_pos);
        VN     = max(max(Vn_neg));
        VP     = max(max(Vn_pos));

        V_neg = (1/VN)*Vn_neg;
        V_pos = (1/VP)*Vn_pos;
    end

    % Store matrices in cell array
    XC(ii,1) = {X};
    IC(ii,1) = {I};

    DC(ii,1)    = {D};
    D_HYD(ii,1) = {D_hyd};
    D_NEG(ii,1) = {D_neg};
    D_POS(ii,1) = {D_pos};

    VC(ii,1)    = {V};
    V_HYD(ii,1) = {V_hyd};
    V_NEG(ii,1) = {V_neg};
    V_POS(ii,1) = {V_pos};

    CO_NEG(ii,1) = {CO_neg};
    CO_POS(ii,1) = {CO_pos};

end
return
```

```
function rect_linear_plot(n,mmin,mmax,epsi,norm)
%=========================================================================
% RECT_LINEAR_PLOT(n,mmin,mmax,epsi): plots the eigenvalues and positive
% and negative acoustic amplitudes for a two-dimensional rectangular duct
% with a linear flow distortion using scatter plots.
%
% INPUT
% n:        radial mode order n
% mmin:     lower bound circumferential mode order m
% mmax:     upper bound circumferential mode order m
% epsi:     flow distortion factor
% norm:     normalization 1 - normalizes individual eigenvectors
%           normalization 2 - normalizes all eigenvectors together
%
% OUTPUT
% figure 1: eigenvalues all modes
% figure 2: amplitudes belonging to negative acoustic m-modes (upstream)
% figure 3: amplitudes belonging to positive acoustic m-modes (downstream)
%=========================================================================

format long

% Range and central mode number
r  = mmin:mmax;
MM = ((mmax-mmin)/2)+1;
m  = (mmax+mmin)/2;

% Calculate eigenvalue and eigenvector data
[XC,IC,DC,D_NEG,D_POS,D_HYD,VC,V_NEG,V_POS,V_HYD,CO_NEG,CO_POS]=...
    rect_linear(n,mmin,mmax,epsi,norm);
```

```
%% Eigenvalues

% All modes
figure(1);clf(1);
for ii=1:n
    plot(real(D_HYD{ii,1}),imag(D_HYD{ii,1}),'r+','MarkerSize',10,...
        'Linewidth',2);
    hold on
    plot(real(D_POS{ii,1}),imag(D_POS{ii,1}),'bo','MarkerSize',10,...
        'Linewidth',2);
    plot(real(D_NEG{ii,1}),imag(D_NEG{ii,1}),'bx','MarkerSize',10,...
        'Linewidth',2);

    legend('hydrodynamic modes','positive acoustic modes',...
        'negative acoustic modes',4);
    xlabel('\Re(\lambda)');ylabel('\Im(\lambda)');
    %axis([-2 3 -0.2 0.2]);
end
grid on
```

```
%% Amplitudes - scatter

% Negative amplitudes
figure(2);clf(2)
for ii=1:n

    plottype=n;
    switch plottype
        case {1,2}
            pp(ii) = subplot(n,1,ii);imagesc(mmin,mmin,V_NEG{ii,1});
        case {3,4}
            pp(ii) = subplot(2,2,ii);imagesc(mmin,mmin,V_NEG{ii,1});
```

```
        case {5,6}
            pp(ii) = subplot(2,3,ii);imagesc(mmin,mmin,V_NEG{ii,1});
        case {7,8,9}
            pp(ii) = subplot(3,3,ii);imagesc(mmin,mmin,V_NEG{ii,1});
        otherwise
            ii = n;
            pp(ii) = subplot(1,1,1);imagesc(mmin,mmin,V_NEG{ii,1});
            disp('Figure 4: only highest n mode is plotted');
            break;
    end

    xlabel('mode order m');ylabel('mode order m');
    title(['n=',int2str(ii),', cut-off if m>=',int2str(CO_NEG{ii}+mmin)])
    line([CO_NEG{ii}+mmin-0.5,CO_NEG{ii}+mmin-0.5],[mmin-1,...
        length(V_NEG{ii,1})+mmin+1],'Linewidth',2,'Color','k');
end

% Create colorbar (works for n<10 only!)
cb = colorbar;
set(cb,'Position',[0.91 0.11 .025 .815])
if n<=9
    for jj=1:n
        pos = get(pp(jj), 'Position');
        set(pp(jj), 'Position', [pos(1) pos(2) 0.85*pos(3) pos(4)]);
    end
end

% Positive amplitudes
figure(3);clf(3)
for ii=1:n

    plottype=n;
    switch plottype
        case {1,2}
            pp(ii) = subplot(n,1,ii);imagesc(mmin,mmin,V_POS{ii,1});
        case {3,4}
            pp(ii) = subplot(2,2,ii);imagesc(mmin,mmin,V_POS{ii,1});
        case {5,6}
            pp(ii) = subplot(2,3,ii);imagesc(mmin,mmin,V_POS{ii,1});
        case {7,8,9}
            pp(ii) = subplot(3,3,ii);imagesc(mmin,mmin,V_POS{ii,1});
        otherwise
            ii = n;
            pp(ii) = subplot(1,1,1);imagesc(mmin,mmin,V_POS{ii,1});
            disp('Figure 4: only highest n mode is plotted');
            break;
    end

    xlabel('mode order m');ylabel('mode order m');
    title(['n=',int2str(ii),', cut-off if m>=',int2str(CO_NEG{ii}+mmin)])
    line([CO_POS{ii}+mmin-0.5,CO_POS{ii}+mmin-0.5],[mmin-1,...
        length(V_POS{ii,1})+mmin+1],'Linewidth',2,'Color','k');
end

% Create colorbar (works for n<10 only!)
cb = colorbar;
set(cb,'Position',[0.91 0.11 .025 .815])
if n<=9
    for jj=1:n
        pos = get(pp(jj), 'Position');
        set(pp(jj), 'Position', [pos(1) pos(2) 0.85*pos(3) pos(4)]);
    end
end
```

```
function rect_linear_plotbar(n,mmin,mmax,epsi,norm)
%=========================================================================
% RECT_LINEAR_PLOTBAR(n,mmin,mmax,epsi): plots the eigenvalues and positive
% and negative acoustic amplitudes for a two-dimensional rectangular duct
% with a linear flow distortion using bar plots.
%
% INPUT
% n:        radial mode order n
% mmin:     lower bound circumferential mode order m
% mmax:     upper bound circumferential mode order m
% epsi:     flow distortion factor
% norm:     normalization 1 - normalizes individual eigenvectors
%           normalization 2 - normalizes all eigenvectors together
%
% OUTPUT
% figure 1: eigenvalues all modes
% figure 2: eigenvalues central m-mode
% figure 3: amplitudes belonging to negative, central acoustic m-mode
% figure 4: amplitudes belonging to positive, central acoustic m-mode
% figure 5: amplitudes belonging to negative acoustic modes
% figure 6: amplitudes belonging to positive acoustic modes
%=========================================================================

format long

% Range and central mode number
r  = mmin:mmax;
MM = ((mmax-mmin)/2)+1;
m  = (mmax+mmin)/2;

% Calculate eigenvalue and eigenvector data
[XC,IC,DC,D_NEG,D_POS,D_HYD,VC,V_NEG,V_POS,V_HYD,CO_NEG,CO_POS]=...
    rect_linear(n,mmin,mmax,epsi,norm);
```

```
%% Eigenvalues

% All modes
figure(1);clf(1);
for ii=1:n
    plot(real(D_HYD{ii,1}),imag(D_HYD{ii,1}),'r+','MarkerSize',10,...
        'Linewidth',2);
    hold on
    plot(real(D_POS{ii,1}),imag(D_POS{ii,1}),'bo','MarkerSize',10,...
        'Linewidth',2);
    plot(real(D_NEG{ii,1}),imag(D_NEG{ii,1}),'bx','MarkerSize',10,...
        'Linewidth',2);

    legend('hydrodynamic modes','positive acoustic modes',...
        'negative acoustic modes',4);
    xlabel('\Re(\lambda)');ylabel('\Im(\lambda)');
    axis([-2 3 -0.2 0.2]);
end
grid on

% Central mode
figure(2);clf(2);
for ii=1:n
    D_NEGn = D_NEG{ii,1};
    D_POSn = D_POS{ii,1};

    plot(real(D_POSn(MM-1,1)),imag(D_POSn(MM-1,1)),'mo','MarkerSize',10,...
        'Linewidth',2);
    hold on
```

```
    plot(real(D_POSn(MM,1)),imag(D_POSn(MM,1)),'bo','MarkerSize',10,...
        'Linewidth',2);
    plot(real(D_POSn(MM+1,1)),imag(D_POSn(MM+1,1)),'go','MarkerSize',10,...
        'Linewidth',2);

    plot(real(D_NEGn(MM-1,1)),imag(D_NEGn(MM-1,1)),'mx','MarkerSize',10,...
        'Linewidth',2);
    plot(real(D_NEGn(MM,1)),imag(D_NEGn(MM,1)),'bx','MarkerSize',10,...
        'Linewidth',2);
    plot(real(D_NEGn(MM+1,1)),imag(D_NEGn(MM+1,1)),'gx','MarkerSize',10,...
        'Linewidth',2);

    legend(['Positive, m=',int2str(m-1)],['Positive, m=',int2str(m)],...
        ['Positive, m=',int2str(m+1)],['Negative, m=',int2str(m-1)],...
        ['Negative, m=',int2str(m)],['Negative, m=',int2str(m+1)],4);
    xlabel('\Re(\lambda)');ylabel('\Im(\lambda)');
    axis([-2 3 -0.2 0.2]);
end
grid on
```

```
%% Amplitudes - bar plots

% Domain
lb = mmin-1;
ub = mmax+1;

% Negative amplitudes central m mode
figure(3);clf(3);
for ii=1:n

    V_NEGn = transpose(V_NEG{ii,1});

    plottype=n;
    switch plottype
        case {1,2}
            subplot(n,1,ii);bar(r,V_NEGn(MM,:));
        case {3,4}
            subplot(2,2,ii);bar(r,V_NEGn(MM,:));
        case {5,6}
            subplot(2,3,ii);bar(r,V_NEGn(MM,:));
        case {7,8,9}
            subplot(3,3,ii);bar(r,V_NEGn(MM,:));
        otherwise
            ii = n;
            subplot(1,1,1); bar(r,V_NEGn(MM,:));
            disp('Figure 3: only highest n mode is plotted');
            break;
    end

    xlabel('mode order m');
    title(['n=',int2str(ii)])
    axis([lb ub 0 1]);
end

% Positive amplitudes central m mode
figure(4);clf(4);
for ii=1:n

    V_POSn = transpose(V_POS{ii,1});

    plottype=n;
    switch plottype
        case {1,2}
```

```
            subplot(n,1,ii);bar(r,V_POSn(MM,:));
        case {3,4}
            subplot(2,2,ii);bar(r,V_POSn(MM,:));
        case {5,6}
            subplot(2,3,ii);bar(r,V_POSn(MM,:));
        case {7,8,9}
            subplot(3,3,ii);bar(r,V_POSn(MM,:));
        otherwise
            ii = n;
            subplot(1,1,1); bar(r,V_POSn(MM,:));
            disp('Figure 4: only highest n mode is plotted');
            break;
    end

    xlabel('mode order m');
    title(['n=',int2str(ii)])
    axis([lb ub 0 1]);
end

% Define ranges to plot
if (mmax-mmin)+1 < 9
    r  = mmin:mmax;
    rr = r-mmin+1;
else
    rr = MM-2:MM+2;
    r  = m-2:m+2;
end

% Negative amplitudes range
figure(5);clf(5);
for ii=1:n

    VN = transpose(V_NEG{ii,1});

    plottype=n;
    switch plottype
        case {1,2}
            subplot(1,1,ii); bar(r,VN(rr,:));
        case {3,4}
            subplot(2,2,ii); bar(r,VN(rr,:));
        case {5,6}
            subplot(3,2,ii); bar(r,VN(rr,:));
        case {7,8,9}
            subplot(3,3,ii); bar(r,VN(rr,:));
        otherwise
            ii = n;
            VN = V_NEG{ii,1};
            subplot(1,1,1); bar(r,VN(rr,:));
            disp('Figure 5: only highest n mode is plotted');
            break;
    end

    title(['n=',int2str(ii)])
    xlabel('mode order m');
    hold on
end

% Positive amplitudes range
figure(6);clf(6);
title('Positive amplitudes');
for ii=1:n

    VP = transpose(V_POS{ii,1});
```

```
        plottype=n;
        switch plottype
            case {1,2}
                subplot(1,1,ii); bar(r,VP(rr,:));
            case {3,4}
                subplot(2,2,ii); bar(r,VP(rr,:));
            case {5,6}
                subplot(3,2,ii); bar(r,VP(rr,:));
            case {7,8,9}
                subplot(3,3,ii); bar(r,VP(rr,:));
            otherwise
                ii = n;
                VP = V_POS{ii,1};
                subplot(1,1,1); bar(r,VP(rr,:));
                disp('Figure 6: Only highest n mode is plotted');
                break;
        end

        title(['n=',int2str(ii)])
        xlabel('mode order m');
        hold on
    end
```

Appendix C

Comparison Rolls-Royce data

This appendix is removed because its content is regarded as strictly confidential to Rolls-Royce. The original version of this appendix is archived at the Rolls-Royce UTC in ISVR Southampton and is only accessible by its members.